ABSTRACT

BLAKE, SAMANTHA LYNN. Dyed Fiber Analysis towards the Development of a LC-MS Comparative Finished Fiber Database for Forensic Purposes. (Under the direction of Dr. David Hinks and Dr. David C. Muddiman).

Traditional forensic fiber analysis includes Fourier transform infrared spectroscopy, microscopy, microspectrophotometry, and sometimes thin layer chromatography of the extracted dye. These methods give information about the fiber type and treatment; however, they lack molecular specificity. The introduction of liquid chromatography-mass spectrometry analysis of the extracted dye information would provide molecular information to the analysis and decrease the chances of incorrect fiber identifications and comparisons. This research includes the construction of a dye proof-of-principle database containing 50 different dyes and its application to unknown dyes and degraded dyes.

The unknown dyes that were analyzed were searched against the proof-of-principle database and correctly identified using the Agilent Qualitative Analysis B.04 software. Another method using k-NN analysis after pretreatment of the database dyes by principle component analysis also accurately identified unknown dyes. A selection of the dyes studied were exposed to UV light for a defined time period then analyzed to determine the database applicability on degraded samples. After degradation of the dye molecule due to the exposure to UV light, enough dye was present in the fibers to get an accurate identification from the dye database for all of the dyes studied, except for CI Acid Green 16, a triphenyl-methane dye that is known to have poor lightfastness. This helps to validate the creation and use of the database for forensic purposes due to the exposure of the fibers of interest to environmental conditions, such as sunlight.

The ability of two instrument platforms to analyze small molecules was also compared. Color Index Disperse Yellow 42 (DY42), a high-volume disperse dye for polyester, was used to compare the capabilities of the LTQ-Orbitrap XL and the LTQ-FT-ICR with respect to mass measurement accuracy (MMA), spectral accuracy, and sulfur counting. The results of this research will be used in the construction of a dye database for forensic purposes; the additional spectral information will increase the confidence in the identification of unknown dyes found in fibers at crime scenes.

Initial LTQ-Orbitrap XL data showed MMAs greater than 3 ppm and poor spectral accuracy. Modification of several Orbitrap installation parameters (e.g., deflector voltage) resulted in a significant improvement of the data. The LTQ-FT-ICR and LTQ-Orbitrap XL (after installation parameters were modified) exhibited MMA $\leq$3 ppm, good spectral accuracy (χ^2 values for the isotopic distribution $\leq$2), and were correctly able to ascertain the number of sulfur atoms in the compound at all resolving powers investigated for AGC targets of 5.00×10^5 and 1.00×10^6.

Dyed Fiber Analysis towards the Development of a LC-MS Comparative Finished Fiber Database for Forensic Purposes

by
Samantha Lynn Blake

A thesis submitted to the Graduate Faculty of
North Carolina State University
in partial fulfillment of the
requirements for the degree of
Master of Science

Chemistry,
CoMajor Textile Chemistry

Raleigh, North Carolina

2013

APPROVED BY:

_____	_____
Dr. David Hinks Committee Co-Chair	Dr. David C. Muddiman Committee Co-Chair
_____	_____
Dr. Keith R. Beck	Dr. Morteza Khaledi

_____
Dr. Maria Oliver-Hoyo

BIOGRAPHY

Samantha Lynn Blake grew up in Salem, Ohio with her mother and sister Sara. She attended college at Ohio University in Athens, Ohio where she earned a Bachelors of Science degree in Forensic Chemistry with a minor in Biology. After graduating from Ohio University, she moved south to Raleigh, North Carolina to attend graduate school at North Carolina State University to earn her Master of Science degree in Chemistry with a CoMajor in Textile Chemistry. On April 20, 2013, Samantha married her husband Brent in Raleigh, NC; where they still reside with their dog, Colby.

TABLE OF CONTENTS

LIST OF TABLES

LIST OF FIGURES

Chapter 1. Introduction

1.1 Purpose

The effectiveness of fibers, a type of trace evidence, in the courtroom depends on the certainty to which they can be traced back to its source using their physical and chemical characteristics. Isolation and identification of fibers are important to the forensic community because of their ease of transfer to the crime scene and potential to provide meaningful insight into the location of the crime or event. Fibers are a common type of trace evidence found at crime scenes with as many as 100-10,000 fibers being transferred by the act of sitting on a seat *(1)* and were key evidence in the convictions of Ted Bundy and Wayne Williams as well as many others *(2)*. In both cases, the ability to identify fibers found on the victims and match them back to a known source proved invaluable for the prosecution. With the current emphasis on DNA analysis in forensics, much work is being done to prove that fibers can still offer valuable insight in the courtroom *(3)*. The purpose of this work is to start the construction of a Liquid Chromatography-Mass Spectrometry (LC-MS) database of dyes extracted from textile fibers. The database will provide mass spectra of known dyes to forensic laboratories for comparison to questioned fibers found at crime scenes.

1.2 Research Objective

The objective of this research is to create a comparative LC-MS dyed fiber database for use in forensic cases. The database would initially consist of automotive fibers from a variety of vehicles of different makes and models and will eventually branch out to other fiber types. The experiments involved in this research include:

1. Comparison of the analysis capability of the LTQ-FT-ICR and the LTQ-Orbitrap XL in regards to the sulfur [M+2] isotopic peak and the whole isotopic distribution generated by C.I. Disperse Yellow 42.
2. Development of a fifty acid dye example database consisting of LC-MS data from raw dye powders. Use of the database to accurately identify ten unknown dyes (five dyes from the database and five dyes not included in the database) will be examined.
3. LC-MS analysis of acid dyes extracted from nylon fibers after photo-degradation to simulate the exposure of fabrics to UV light over time.

The overall objective of this research is to show the advantages that an LC-MS comparative dye database would contribute to the forensic field when used in conjunction with current fiber analysis techniques.

Chapter 2. Literature Review

2.1 Acid Dyes

Dyes are classified according to their chemical class (*e.g.*, azo, anthraquinone, triphenylmethane) or application method. Acid dyes are typically applied to nylon, wool, and silk fibers under acidic conditions, which generate protonated amines in the fibers, and establish ionic bonds between the negatively charged, sulfonated dyes and the protonated fibers *(4)*. There are approximately 2354 acid dyes in the Colour Index that are often used in combination to give fabrics the desired color and within the acid dye class there are several subgroups based on the chromophore in the dye molecule. The most common chromophores

found in acid dyes are azo, anthraquinone, and triphenylmethane. Less common systems are based on pyrazalone, hydrazones, azine, nitrodiphenylamine, and phthalocyanine. Azo dyes are highly versatile and can be used to produce a large color range while the other dye chemical classes are more restricted. For example, anthraquinoid derivatives are mostly red to blue and have high washfastness, while xanthene-based dyes tend to be bright red-pink *(4)*. Dyes vary significantly in their chemistries helping them to impart a wide range of colors on many different fiber types.

2.2 Forensic Dye Analysis

Current forensic dyed fiber analysis methods involve various levels of analytical tools yielding information that is used in combination to maximize the usefulness of the analysis *(5)*. Identification of the dye found in colored fibers in addition to specific fiber properties adds another level of discrimination to fiber analysis and the use of mass spectrometry (MS) introduces molecular specificity to the analysis. **Figure 1***(6)* shows a flow chart of methods used during forensic fiber analysis. The nature of the fibers, whether natural or man-made, along with the starting material of the evidence, fiber or fabric etc, determines the combination and order of the analysis methods utilized. When choosing target fibers, fibers of interest that will be used as evidence, investigators look for characteristics that will help increase the discriminatory value of the fiber, for example, the occurrence of the fiber in the textile industry and the physical characteristics such as coarseness and fluorescence *(6)*. Common fibers are considered to be less useful; however, a common fiber type, such as a blue polyester fiber, has been found to be useful when found in an unusual environment *(1)*.

All aspects must be considered when choosing the optimal target fibers to associate a suspect with a crime.

Microscopy *(7-12)*, infrared spectroscopy (IR) *(13-25)*, thin-layer chromatography (TLC) *(26-36)*, and UV-visible microspectrophotometry (MSP) *(32, 35, 37-40)* have all been researched extensively for their application to forensic fiber analysis and are typically used in investigations. Raman spectroscopy *(25, 41-49)* has also been investigated for potential use in forensic fiber analysis but has not yet been utilized in a majority of forensic laboratories for fiber analysis purpose. The development of automated extraction and analysis techniques is an attractive possibility for use in the field during evidence collection. The automation of extraction of dyes from fibers *(50)* for analysis by capillary electrophoresis (CE) *(50-56)* has been studied by Morgan and coworkers in hopes that a suitable method will be developed for forensic use. HPLC *(57-63)* and MS *(54, 55, 60-68)* analysis methods have also been developed for possible forensic use as well as for historical research.

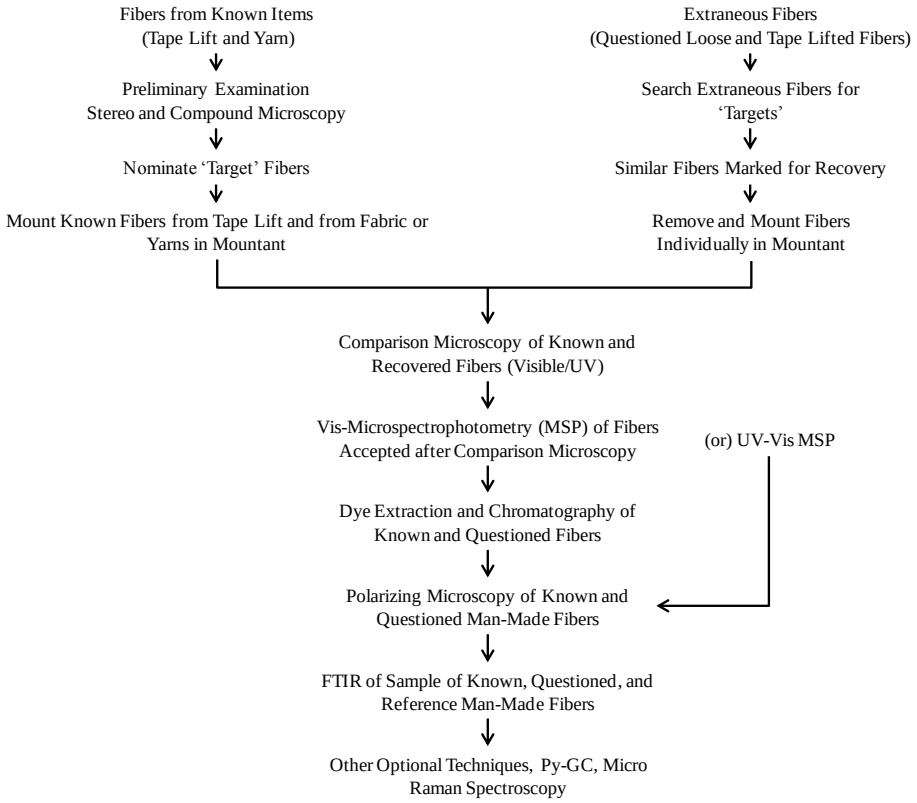

Figure 1. Flow diagram for forensic fiber examination.

The forensics field has been heavily focused on DNA analysis because of its high discriminating capability which has prompted labs to investigate the individuality of fibers and their significance as evidence *(1, 8, 40, 69-80).* Biermann and coworkers studied diameter, cross section, fluorescence, delustrant particle size, birefringence, and the UV-Vis spectra of 255 blue polyester samples and found 3 random matches *(1).* In theory, the addition of LC-MS to the analysis protocol would reduce this number to zero random matches making it an invaluable tool for forensic analysis where a high level of discrimination is important.

The current required analytical tests for fiber evidence are outlined in the *Forensic Fiber Examination Guidelines* put together by the Scientific Working Group on Materials Analysis (SWGMAT). A combination of methods in an order that maximizes accuracy, precision, and production is required. There are two purposes to forensic fiber analysis; identification of questioned fibers and comparison of questioned fibers to known fibers *(81)*. The purpose of the analysis helps to determine the methods and techniques employed for the analysis.

2.2.1 Microscopy

Stereomicroscopy, comparison microscopy, PLM, fluorescence microscopy, and MSP methods are commonly employed for analysis of dyed fibers. Each microscope is used to determine a different property of the fiber to be used to get the highest discrimination capability possible for the identification and comparison of questioned samples.

Stereomicroscopy is a lower magnification technique but allows for large sample sizes typically encountered during the fiber recovery process from tape and large pieces of evidence *(6)*. Once the target fibers are recovered using the stereomicroscope with both reflected and transmitted light, other analytical methods are employed to study the fiber.

Comparison microscopy is used in forensic fiber examination for side by side comparison of known and questioned fibers for points of similarity and points of difference *(6)*. A comparison microscope consists of two compound microscopes connected by an optical bridge. They can also be fitted with addition elements, such as a polarizing light microscopy (PLM) element, to provide a more thorough examination of fiber properties.

Microscopy is used to view the physical properties of the fiber that are present from manufacturing as well as from use. Man-made fibers are typically smooth and uniform; however, wear patterns and signs of age can provide valuable insight into the fiber history. Some physical characteristics that can be determined are diameter, cross-sectional shape, surface features, fluorescence (using fluorescence microscopy), internal detail, and color.

PLM is used to determine the optical properties of questioned fibers; which in most cases are sufficient to determine fiber type. Optical properties come from the chemical composition of the fibers or changes in orientation and spacing of constituents that occur during spinning and treatment of the fibers *(81)*. PLM is used to determine properties such as sign of elongation, quantitative birefringence, isotropic refractive index (n_{iso}), and the refractive index for light vibrating in a plane parallel to the fiber ($n_{\parallel}$) or in a plane perpendicular to the fiber ($n_{\perp}$) *(81)*.

2.2.2 UV-visible Microspectrophotometry (MSP)

In forensics, UV-visible MSP is a quick non-destructive method to analyze small colored fibers for comparison purposes by recording the UV-visible spectrum without having to remove the fiber from the microscope slide. UV-visible spectroscopy is used to study conjugated systems making it an ideal method for dye analysis because of the extended conjugation systems in dye molecules needed to produce color. It is used for the study of metemeric fibers; fibers that appear to be the same color but were created using different dyes. MSP is a single beam instrument but is able to store incident light intensity to use for background subtraction from the light transmitted through the fiber, allowing it to perform as

a double beam instrument *(81)*. Grieve and coworkers investigated the percentage of matching spectra of blue, red, and black dyed cotton and found that within the red and black color classes less than 1.5% of spectra matched and only 0.2% of the blue spectra matched *(32)*. Macrae and coworkers also investigated the discrimination capability of MSP but focused on wool fibers. In their comparison of blue wool fibers, they found that comparison microscopy with white light only offered a discrimination of 47% but the discrimination capability of MSP was 99%, the same as their findings for TLC *(37)*; however, MSP is nondesctructive and can be used on fibers with low dye concentrations when extraction and analysis via TLC is not possible.

2.2.3 Infrared (IR) and Raman Spectroscopy

IR is used for the identification of the fiber polymer through investigation of the vibrational frequencies of the molecules after irradiation in the IR region. FT-IR has increased the speed and sensitivity of IR spectroscopy making it a useful and often employed tool in forensic science. FTIR databases have been developed for simple polymer identification in the forensics lab *(13, 15)*. Grieve and coworkers studied FTIR spectra of dyed acrylic fibers and were able to determine absorptions of the dyes along with the characteristic polymer absorptions *(21)*.

Resonance Raman works by using a laser excitation in resonance with the dye molecule to cause molecular vibrations. It is an attractive tool for forensic dyed fiber analysis because it is more sensitive and specific than IR spectroscopy and can also detect dyes in small concentrations. Surface enhanced resonance Raman scattering (SERRS) was

used for the in-situ detection of reactive dyes at picrogram concentrations on cotton after digestion for 21 hours *(41, 44)*. Raman microprobe spectroscopy was successfully utilized for fiber polymer characterization without sample preparation; however, the dye needed to be extracted to obtain spectra for both the dye and the polymer *(43)*. Resonance Raman has been successfully employed for the detection and discrimination black dyes of different textile types *(46, 48)* and of reactive dyes on cotton *(42)*. Raman spectroscopy has potential for investigation of dyed fibers for forensic purposes; however, much research and standardization of methods need to be done.

2.2.4 Thin Layer Chromatography

TLC offers the advantages of convenience, the ability to separate multiple samples on the same plate, and easy detection through the addition of colored reagents. In TLC the samples are spotted on a plate coated with an adsorbent material that acts as the stationary phase, usually silica gel, and placed vertically in a chamber with a solvent or solvent mixture, depending on the chemical nature of the dye being studied, which acts as the mobile phase. The mobile phase travels up the TLC plate via capillary action and the analytes of the sample undergo separation based on their different migration rates due to interactions with the stationary phase and the mobile phase. The distance the spot travels from its starting position divided by the total distance the mobile phase traveled gives the capacity factor (k') that can be used for compound identification *(82)*. The k' of known and questioned samples can be compared to help in the identification of evidence.

TLC is used in forensic science for the analysis of dyes extracted from forensic fiber evidence when comparison microscopy and microspectrophotometry of the visible range are not able to discriminate between fibers of interest *(83)*. TLC cannot be used for forensic use in the case of sample limited evidence and can only be used for comparisons to a known fiber. Beattie and coworkers developed methods for the extraction and TLC analysis of acid, disperse, and basic dyes from nylon, polyester, and polyacrylonitrile fibers finding them useful only in a comparison capacity in the forensic field *(26, 29)*. TLC was used to compare historic Grübler dyes to their modern day counterparts to ensure correct labeling and purity for future manufacturing purposes *(36)*. Their findings highlight the issue of continuity between different dye manufacturers across the globe which could introduce problems in the development of a dye database if there are dyes that are mislabeled or have excessive impurities.

2.2.5 Pyrolysis-Gas Chromatography

Pyrolysis involves the thermal decomposition of analytes into molecular fragments characteristic of the initial fiber. Pyrolysis can be used in conjunction with GC and a variety of detectors depending on the desired information. Detectors used with Py-GC include flame ionization (FID), alkali flame ionization (AFID), flame photometric (FPD), electron capture (ECD), and MS *(6)*. The detectors provide retention times of characteristic components that can be identified using databases or known fiber samples. MS detectors offer higher sensitivity and provide the most information out of the detectors mentioned because they introduce molecular specificity of the components *(6)*.

2.2.6 High Performance Chromatography and Capillary Electrophoresis

HPLC methods have been developed and successfully utilized for the analysis of dyes on textile fibers for forensic use. HPLC is a quantifiable method that also could be utilized for the construction of databases making it advantageous over TLC. Methods have been developed for the analysis of acid *(57)*, basic *(58)*, and disperse dyes; however, analysis of acid dyes typically involves the use of ion pairing agents rendering it useless for MS detection. Mottaleb and coworkers attempted HPLC-FTIR with a thermospray interface for dye analysis to produce FTIR chromatograms and IR spectra but found the technique lacked sensitivity *(59)*. HPLC and CE separation conditions vary based on the chemical composition of the analytes of interest. Different experimental conditions have been developed for each dye type for both HPLC; however, standardized conditions have still not been established.

CE separates small volumes of ionic species in a capillary filled with buffer solution with an applied high voltage filled, based on their charge to mass ratio. When utilized with MS detection the capillary effluent goes directly into the electrospray interface *(82)*. CE-MS with negative ion electrospray ionization has been successfully used to identify anionic metalized azo and formazan dyes *(51)*. Morgan and coworkers have developed automated extraction methods with different solvent conditions suitable for each dye type for analysis via CE. Diode- array detection (DAD) was used for the dye types *(50, 56)*; however, when investigating small sample size DAD was not deemed useful, instead MS detection coupled with CE was used for sample sizes as small as 2 mm fibers *(55)* and was also successful in the analysis of natural dyes *(52)*.

2.2.7 Mass Spectrometry

MS is a powerful potential tool for forensic analysis of dyes extracted from textiles because of its high sensitivity and reproducibility as well as the molecular level of information it provides. There has also been discussion of the usefulness of an MS dye database for forensic purposes *(60, 61)*. Many research groups have been successful at the HPLC-MS analysis of fiber dyes. Tuinman and coworkers analyzed acid dyes extracted from nylon via MS using direct infusion methods for comparison of dyes while also utilizing MS/MS for dyes of the same *m/z (65).* HPLC of acid dyes has been difficult and typically requires mobile phase additives that are not compatible with MS because they cause signal suppression. HPLC-MS analysis has been achieved through removal of the additives before injection into the MS *(63)* while some groups have reported the use of triethylammonium acetate to be successful in small quantities *(60).* MALDI –MS has also been considered for dye analysis because of its easy sample prep and ability to be used with dyes that are insoluble *(66, 68)*. While there is still work to be done in the development of the analysis of dyes by MS, there is much potential for the development of a database that could be utilized across forensic laboratories.

2.3 Instrumentation

2.3.1 High-Performance Liquid Chromatography

Liquid chromatography (LC) began in the 1905 with classical column chromatography separation of colored pigments by Michael Tswet *(84).* In column chromatography, solvent flow through the column is due to gravity and fractions are

collected as they elute from the end of the column. Traditional column chromatography is time consuming and requires a new column be used for every sample *(84)*. Paper chromatography was invented in 1943 by A.J.P. Martin and the addition of a thin layer of silica over the chromatography paper or glass plate led to the development of thin-layer chromatography (TLC) *(84)*. The next stage of the development of LC was realized when the first high-performance liquid chromatography (HPLC) paper appeared in 1966 and by 1971 the first HPLC book was published *(84)*.

HPLC is a separation technique that involves a liquid mobile phase and a stationary phase. The mobile phase can be manipulated easily to accommodate a variety of chemical compositions. Samples need not be volatile to undergo HPLC separation, allowing a wider range of compounds to be analyzed than with GC *(84)*. In reverse phase HPLC, the sample is injected via an autosampler into a column along with a constant flow of solvent. A pump keeps the solvent flow rate constant while the analytes of interest partition between the mobile phase and stationary phase undergoing separation. The detector plots out the results as a function of time *(84)*. **Figure 2** shows a schematic of the HPLC system used for this research. The black arrow marks the flow of solvent through the system.

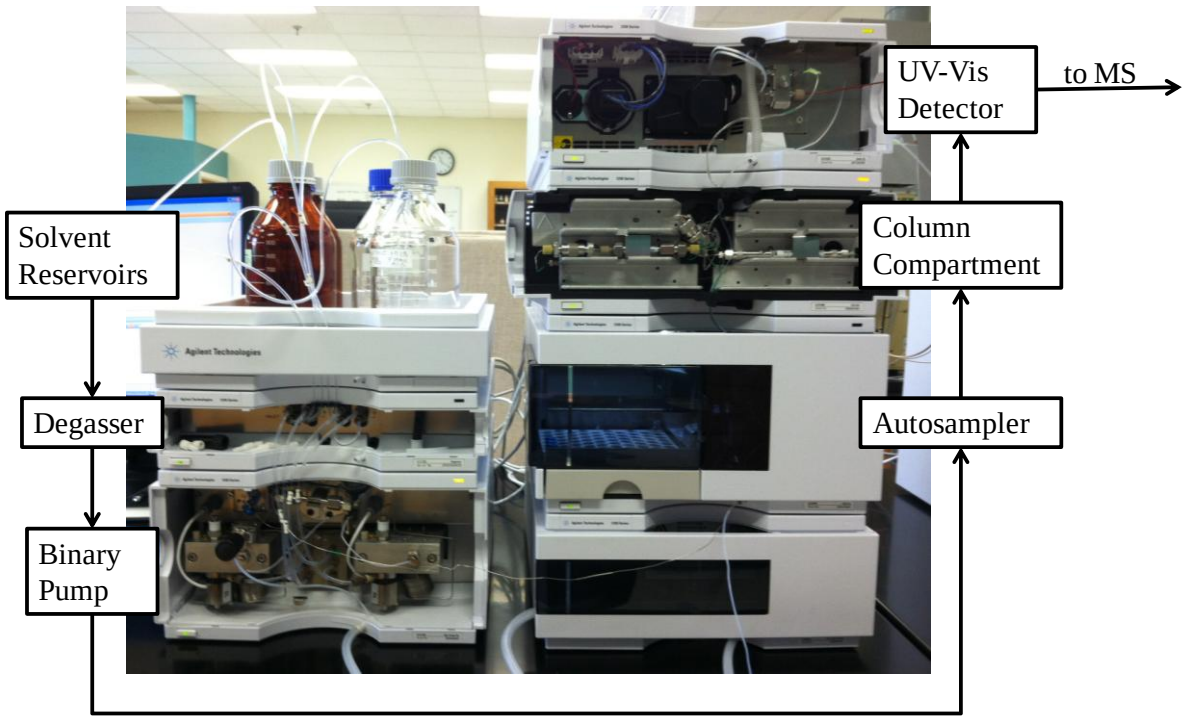

Figure 2. HPLC schematic

Mass transport occurs by way of two mechanisms through the column; mobile phase flow and molecular diffusion. The mobile phase flow carries solutes through the column while individual analyte molecules diffuse in and out of the stationary phase. All analytes spend the same amount of time in the mobile phase; therefore, separation occurs through the differences in the amount of time the analytes spend in the stationary phase *(84)*. The stationary phase is chosen based on the compounds being separated. The two main forms of HPLC are Reverse Phase HPLC (RPLC) and Normal Phase HPLC (NPLC). This review will focus on RPLC.

Reverse phase liquid chromatography (RPLC) is used for separation of moderately polar to nonpolar compounds. In RPLC, the mobile phase is more polar than the stationary

phase and compounds are eluted from the column in order of decreasing polarity *(84)*. Coupling of HPLC to MS for acid dye analysis has been difficult due to the need for ion-pairing reagents that are not volatile and therefore not compatible with MS detection *(63)*. The use of volatile amines has proven successful when used in small concentrations (< 2.5 mM) to detect aromatic sulfonates in wastewater *(85)* and in the identification of dyes extracted from fibers *(60)*.

2.3.2 Electrospray Ionization

The coupling of HPLC and MS was initially a problem before the development of electrospray ionization (ESI) due to the use of a liquid mobile phase and the involatility of analytes. ESI is a soft ionization method that utilizes a charged capillary to send solvent droplets into an atmospheric pressure region towards a counter electrode *(86)*. As the droplets pass through the atmospheric pressure region, they are desolvated by nitrogen drying gas before entering a high vacuum region and travelling into the mass spectrometer, **Figure 3**. There are four steps that occur during the ESI process; droplets of HPLC mobile phase and analyte are formed then become charged, followed by desolvation and the formation analyte ions *(87)*. There are two main theories about the chemistry taking place during this process, the charge residue model and the ion evaporation model *(87)*.

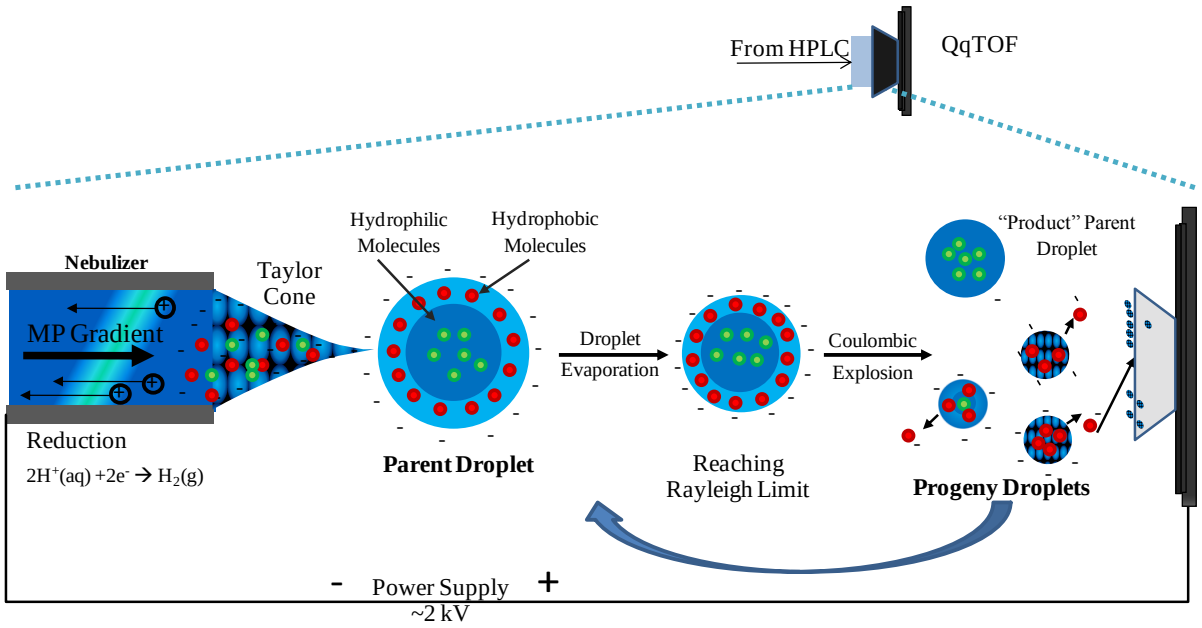

Figure 3. Negative ESI schematic.

The charge residue model proposes the existence of an ultimate droplet that contains only one species. The solvent evaporates and the surface energy of the droplet decreases until the Rayleigh limit is reached and the drops undergo repeated Coulombic fissions until only the "ultimate droplet", consisting of a gas phase analyte molecule and charge originating from surface charge of the evaporated droplet, remains *(88)*. The ion evaporation model theorizes that as the solvent evaporates, the charges cause electrostatic repulsion and product droplets are formed. The product droplets continue to undergo evaporation until the Rayleigh limit is reached and smaller droplets containing a few molecules and a single charge are ejected and travel to the MS *(89)*. Both models have been researched extensively finding that the ion evaporation model is ideal for the explanation of small molecules but the charge residue model is more plausible for macroions such as proteins *(90)*.

2.3.3 Quadrupole-Time-of-Flight

Q-TOF is a triple quadrupole mass spectrometer with the third quadrupole replaced by a time-of-flight (TOF) mass analyzer. The first quadrupole is mass resolving followed by an r.f. only hexapole collision cell that leads into a TOF mass analyzer. When used in single MS mode the first two quadrupoles act as ion focusing and the ions are detected in the TOF. TOF is a kinetic energy dependent mass analyzer that offers the advantages of high sensitivity, high mass resolution, and high mass accuracy. Flight times are measured in microseconds with nanosecond differences between ions of the closest *m/z*. In single MS, mode the TOF offers 2 ppm mass accuracy and femtomole to attomole limits of detection. The ability to multiply charge the ions allows the instrument to have an unlimited mass range*(86)*.

Equation 1. Relationship between flight time and *m/z.*

$$t = \Delta x \sqrt{\frac{m}{2zeU_{ex}}}$$

In TOF, flight times are proportional to *m/z*, **Equation 1***(86),* where t is ion flight time, m is mass, z is charge state of the ion, e is electron charge, and U_{ex} is the extraction voltage. The reflectron was added to overcome any kinetic energy differences that would alter the time of flight to *m/z* proportionality. The reflectron is a set of lenses with a voltage gradient that acts as an ion mirror, at the end of the flight tube used to help diminish the kinetic energy spread of the ions*(86)*. The voltage gradient slows down the ions then pushes

them back out with the same speed with which they entered; however, the ions with greater kinetic energies penetrate farther into the field causing them to have a longer flight path than the ions with less kinetic energy*(86)*. In **Figure 4,** the flight paths of two ions of the same *m/z* are shown. The ion depicted by the circle leaves the pulse plate with a higher kinetic energy than the ion depicted by the square. Both ions travel the flight tube and enter the reflectron; however, ion with the higher kinetic energy penetrates farther into the reflectron before it changes directions and is ejected at the same speed at which it entered enabling it to catch up with the ion of lower initial kinetic energy at the detector and allowing both ions to be detected at the same time.

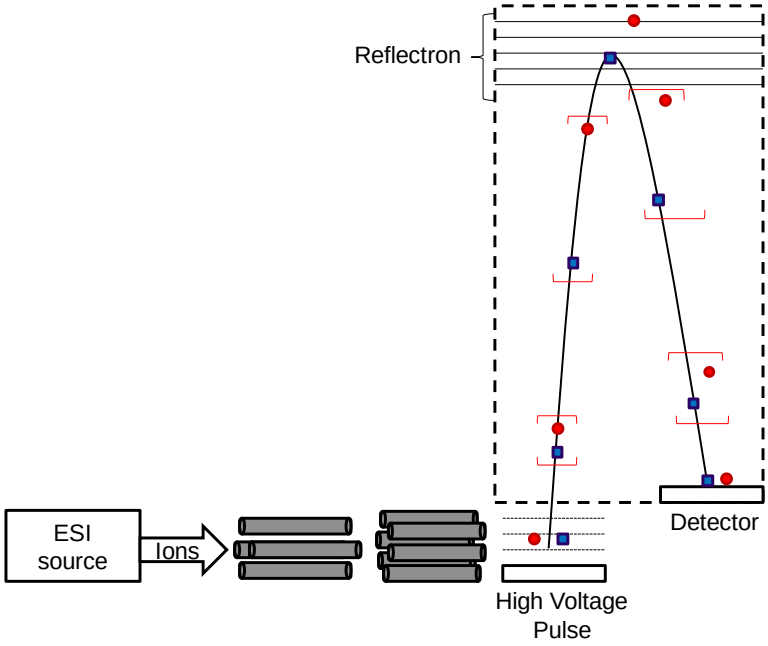

Figure 4. Quadrupole Time-of-Flight Mass Spectrometer schematic

The TOF is equipped with orthogonal acceleration, which enables it to be used with the ESI ion source. Without orthogonal acceleration the TOF would not be compatible with

a continuous ion source such as ESI due to the spatial and energy spreads of the ions resulting from the continuous flow ion source *(91)*.

2.3.4 Fourier Transform- Ion Cyclotron Resonance Mass Spectrometry

Fourier transform- ion cyclotron resonance (FR-ICR) is a high resolving power mass spectrometry technique utilizing a uniform magnetic field. Gas-phase ions in the presence of a uniform magnetic field will follow a circular path perpendicular to the direction of the magnetic field at a frequency related to their *m/z (86)*. Two excitation plates, positioned opposite one another, **Figure 5**, irradiate the ions in the ICR cell with a uniform rf only electric field (excitation pulse) at the same frequency as their natural resonance, increasing their orbit and causing phase coherence of ions of the same *m/z*. Two opposite parallel detection plates measure an image current (time-domain signal) that is Fourier transformed into a frequency domain signal, that is converted to mass domain by **Equation 2**, where ω_c is cyclotron frequency, q is charge, B_o is magnetic field, and m is mass *(92)*.

Equation 2. Relation of cyclotron frequency to mass (m) and charge (q) in a uniform magnetic field (B)

$$\omega_c = \frac{qB_o}{m}$$

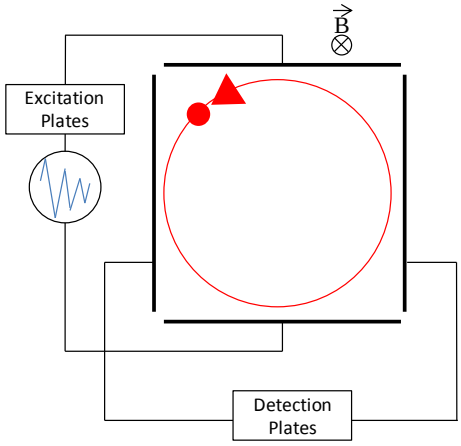

Figure 5. Schematic of an FT-ICR cell.

2.3.5 Orbitrap Mass Spectrometry

The Orbitrap is considered a modified Knight-style Kingdon trap that consists of two coaxial axisymmetric electrodes and an outer barrel shaped surface and an inner spindle shape electrode *(93, 94)*, **Figure 6**. Detection in the Orbitrap is similar to that in FT-ICR; however, it does not use a magnetic field and the ions do not undergo excitation. The ions are electrostatically trapped in the Orbitrap while rotating around the central spindle electrode and oscillating axially. The image current generated by the ions is Fourier transformed to get the axial frequency, which can be converted to *m*/z via **Equation 3** *(95)*.

Equation 3. Relationship between m/z and axial frequency.

$$\omega_a = \sqrt{\frac{k}{m/z}}$$

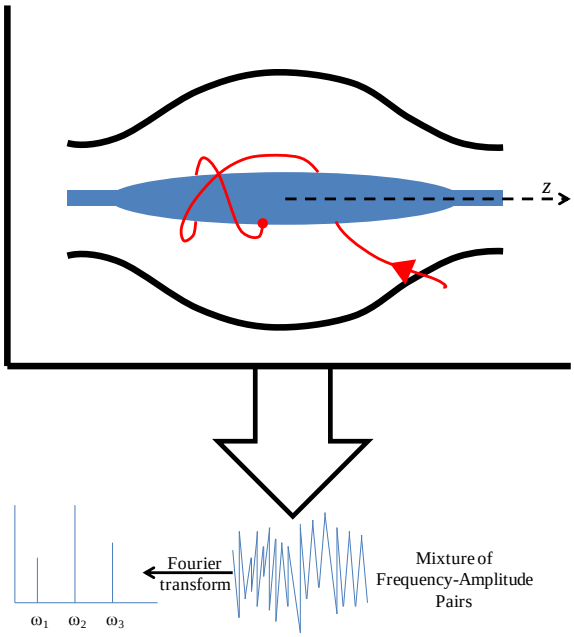

Figure 6. Cut-away view of an Orbitrap an example ion trajectory shown in red.

2.4 Spectral Accuracy and Sulfur Counting

High resolving power (RP) mass spectrometers have the ability to provide high mass measurement accuracy (MMA) which is invaluable in defining the elemental composition of unknowns *(93, 96, 97)*. However, MMA only takes into account the monoisotopic peak, not the entire isotopic distribution. High RP instruments produce spectra that contain useful isotopic information that can be utilized to provide more confident elemental compositions. Isotopic distributions contain several peaks whose relative heights are due to natural isotopic abundances and can be used to aid in the elemental composition determination of an unknown substance *(98)*. For example, the relative abundance of the A+1 peak compared to the monoisotopic peak in conjunction with the natural abundance of the ^{13}C isotope is indicative of the total number of carbons in the compound *(86)*. The relative abundance of

the A+2 peak in the distribution can be used to accurately predict the presence and the number of atoms with A+2 isotopes, such as sulfur, bromine, and chlorine *(98, 99)*.

Spectral accuracy is the ability of the mass spectrometer to correctly measure the isotopic distribution of ions *(100)*. Accurate isotopic ratios are necessary to increase confidence in elemental composition assignments. Isotopic distribution evaluation analyses have been reported in the literature using Orbitrap *(101)* and FT-ICR spectra *(102)* as a way to reduce the number of possible elemental composition assignments for a given species. Junot *et al*. found that absolute ion abundance was the main factor affecting the isotopic distribution and mass accuracy while studying isotopic distributions in the LTQ-Orbitrap *(101)*. They also found that liquid chromatography improved the relative isotopic abundances of the distribution, which is attributed to decreasing the number of isotopic distributions present *(101)*. Stoll *et al.* evaluated different methods, such as calculated double-bond equivalence, ion state, and isotopic distribution simulation and comparison, to compare theoretical and experimental data as a means of narrowing elemental composition assignments *(102)*. In the 25 compounds studied, they found that isotopic distribution evaluation led to a decrease in the number of possible elemental composition assignments for a given species by an average of 90.6% *(102)*. Thus, the accurate measurement of not only the mass (MMA), but also the isotopic distribution can be significantly exploited for the confident identification of elemental compositions in high RP mass analysis.

Using high RP MS, it is also possible to count (in some cases estimate) the number of specific atoms (C, S, Br, Cl, etc.) in a compound through analysis of the A+1 and A+2 isotopic peaks. For example, using the natural abundance of the ^{34}S atom and the relative

height of the resolved doublet at the A+2 peak, the number of sulfurs in a molecule can be determined. The natural abundance of the ^{34}S isotope is 3.976%-4.734%, as reported by NIST *(103)*. When sulfur is present in a compound, high RP MS (≥30,000) is capable of resolving the A+2 peak into a doublet with a mass difference of 0.0109 Da between the peaks. The lighter peak, indicative of the $^{34}S_1$ isotope, has a mass difference of 1.9958 Da from the monoisotopic mass and the heavier peak, indicative of the $^{13}C_2$ isotopic peak, has a mass difference of 2.0067 Da from the monoisotopic mass *(99)*. The relative abundance of the ^{34}S peak in comparison to the monoisotopic peak depends on the number of sulfur atoms present in the compound. For each sulfur present in the compound, the relative abundance of the ^{34}S peak increases by the natural abundance of the ^{34}S isotope. The ability of high RP mass spectrometers to count sulfurs has been studied previously *(104-106)*. Marshall and coworkers used sulfur-counting as a means to characterize the p16 tumor suppressor protein *(104)*, and also later in the study of glycosphingolipids *(106)*. Hoye and coworkers applied sulfur-counting to the study of sea lamprey pheromones *(105)*.

Automatic gain control (AGC) target is a means of controlling the ion population during analysis *(107, 108)*. Higher ion populations increase space charge effects and can lead to decreased MMA; additionally, variable ion populations can allow for variable MMA and spectral accuracy for each individual scan. Thus, AGC allows one to keep the total ion population 'constant' which significantly decreases the analytical variability of the measurement *(109)*.

2.5 Forensic Chemometric Applications

The application of chemometrics has been studied extensively for forensic use. Principal component analysis (PCA) is a statistical method that analyzes variables of multiple samples and reduces them to principle components that can be graphed and analyzed to determine which principle components have the most impact on the data. The number of principal components is equal to the number of descriptors in the data set. The samples are plotted out on the principal components that encompass the greatest amount of variance in the data set *(110)*. PCA can be used in conjunction with cluster analysis and classification algorithms to identify unknowns by mapping their distance in pattern space to known objects. PCA and cluster analysis were used on Raman data of forensic paint samples *(111)*, and narcotics *(112)*. PCA and k-NN were used together to effectively identify heroin batches *(113)*. PCA and K-means have been used in conjunction for the successful evaluation of ball point pen inks analyzed via UV-Vis *(114)*, and HPLC *(115)*, as well as for forensic soil analysis *(114)*.

The analysis of ballpoint pen inks using HPLC and UV-Visible spectroscopy has be successfully used to classify pen type *(115)*. In the analysis of red, black, and blue pens they were most successful with an 87.5% classification of the blue ballpoint pen by using class distances found after PCA analysis; however the addition of LC-MS data to these analyses would increase the correct classification of the pens due to the addition of molecular information *(115)*. PCA and K means cluster analysis were used for the successful identification of 100% of the blue ball-point pen inks studied based on their visible spectra *(114)*. The addition of chemometric methods to dye and ink information would provide the

framework for the development of a database for the identification of dyes found in questioned fibers.

Chapter 3. Spectral Accuracy and Sulfur Counting Capabilities of the LTQ-FT-ICR and the LTQ-Orbitrap XL for Small Molecule Analysis

In Chapter 3, the capabilities of the LTQ-FT-ICR and the LTQ-Orbitrap XL for determination of elemental composition through utilization of MMA, spectral accuracy, and sulfur counting are compared. AGC target and resolving power were varied in both the LTQ-Orbitrap XL and the LTQ-FT-ICR as a means of understanding the capabilities and limitations of the instrumentation pertaining to small molecule analysis. Furthermore, the authors present two separate data sets acquired on the LTQ-Orbitrap XL. The initial data set taken on the LTQ-Orbitrap XL produced spectra with MMA > 2.5 ppm and inaccurate sulfur counting analyses despite the instrument passing all user tuning procedures and being calibrated per the manufacturer specifications. Thus, detailed inspection and manual tuning of the installation parameters by the manufacturer followed, and sub-ppm MMA was achieved in subsequent data acquisition (*vide infra*).

3.1 Experimental

3.1.1 Disperse Yellow 42 Sample Preparation

Color Index (C.I.) Disperse Yellow 42, $C_{18}H_{15}N_3O_4S$, (DY 42), trade name Foron Yellow AS-FL, was obtained from Clariant (Batch CHAA109775) for analysis. To purify the dye powder for analysis, raw dye powder (20 mg) was dissolved in acetone (20 mL) and

brought to a boil while stirring on a hot plate. The sample was filtered hot, and the filtrate was evaporated to dryness. The dried sample was collected for analysis.

Two stock solutions (1 mg/mL) of the purified dye powder were prepared in 50:50 acetonitrile:water. The samples were diluted to 10 µg/mL for analysis on a hybrid linear ion trap, Orbitrap mass spectrometer, LTQ-Orbitrap XL (Thermo Scientific, San Jose, CA) and a hybrid linear ion trap, Fourier transform ion cyclotron resonance mass spectrometer, LTQ-FT-ICR, (Thermo Scientific, San Jose, CA) with a 7 Tesla superconducting magnet.

3.1.2 LTQ- FT-ICR Analysis

The instrument was calibrated per the manufacturer specifications. The 10 µg/mL sample was introduced by direct injection via an in-house nanoESI source. The following instrument parameters were used for all analyses on the LTQ-FT-ICR: capillary voltage and temperature of 42 V and 225°C, respectively, and a tube lens voltage of 120 V. Thirty full range mass spectra (150-2000 *m/z*) were collected at two AGC targets: 5.00×10^5 and 1.00×10^6. The full-width-half-maximum resolving powers (RP_{FWHM} at *m/z*=400) evaluated were 12,500, 25,000, 50,000, 100,000, and 200,000.

3.1.3 LTQ-Orbitrap XL Analysis

The instrument was calibrated per the manufacturer specifications with the lock-mass feature enabled. All instrument parameters were the same as specified for the LTQ-FT-ICR (*vide supra*). The resolving power and AGC target were varied and 30 full range (200-2000

m/z) spectra were collected at each set of conditions. The following RP_{FWHM} at *m/z*=400 were used during the LTQ-Orbitrap XL analysis: 7,500, 15,000, 30,000, 60,000, and 100,000 at *m/z*=400. The same AGC targets were used as with the LTQ-FT analysis.

3.1.4 Data Analysis

The MMA, χ^2 value for the isotopic distribution, and relative abundance of the A+2 sulfur peak were calculated. **Equation 4** is the formula used to calculate the MMA of the monoisotopic peak at each resolving power and AGC target.

Equation 4. MMA formula

$$\mathrm{MMA(ppm)} = \frac{\mathrm{Experimental} - \mathrm{Theoretical}}{\mathrm{Theoretical}} \times 10^6$$

The χ^2 value for the relative abundances in relation to the monoisotopic peak in the isotopic distribution of DY 42 was calculated to quantify spectral accuracy; shown as **Equation 5** *(116)*. The χ^2 value was calculated for each spectrum at each resolving power and AGC target studied.

Equation 5. χ^2 formula

$$\chi^2 = \Sigma \frac{(\mathrm{Observed} - \mathrm{Expected})^2}{\mathrm{Expected}}$$

The number of sulfurs was found by determining the relative abundance of the sulfur peak compared to the monoisotopic peak and multiplying by the ^{32}S:^{34}S natural composition ratio where A+2 and A are the experimenetal peak intensities of the ^{34}S and monoisotopic peak, respectively. $^{32}S_{Theoretical}$ and $^{34}S_{Theoretical}$ are the natural isotopic compositions as reported by NIST of the ^{32}S and ^{34}S, respectively.

Equation 6. Formula used to calculate the number of sulfurs in the compound using the isotopic peak height.

$$\frac{A+2_{Experimental}}{A_{Experimental}} \times \frac{^{32}S_{Theoretical}}{^{34}S_{Theoretical}} = \#\ of\ Sulfurs$$

3.2 Results and Discussion

Two data sets will be discussed for the LTQ-Orbitrap XL in comparison to a data set produced by the LTQ-FT-ICR. The initial data set for the LTQ-Orbitrap XL produced results that are not consistent with the potential specifications reported for an Orbitrap instrument by the manufacturer (e.g. sub-ppm MMA). Additionally, despite passing all user tuning methods and being calibrated per the manufacturer specifications, this group has observed sub-par MMA for this instrument since installation. Furthermore, before the installation parameters were adjusted, sulfur counting experiments in the LTQ-Orbitrap XL did not produce the correct number of sulfurs for a standard molecule. Thus, in a personal communication with Alexander Makarov *(117)*, he immediately concluded that the Orbitrap was not performing optimally upon assessment of the data. During his assessment, he manually tuned specific installation parameters of the instrument. These installation

parameters are not included in the user tune method, and it is not recommended that these parameters be changed by anyone other than a manufacturer engineer. The parameters that were changed include deflector voltage on the Orbitrap and the injection level of the central electrode along with minor adjustments to the lens voltages and pulse voltages on the C-trap. Upon manual optimization of these installation parameters, the second set of data from the LTQ-Orbitrap XL was collected, which produced significantly higher quality data with respect to MMA and spectral accuracy.

Figure 7a, **Figure 7b**, and **Figure 7c** are example spectra of each data set for DY 42 produced by LTQ-FT-ICR, LTQ-Orbitrap XL (before manual adjustment of the installation parameters), and LTQ-Orbitrap XL (after manual adjustment of the installation parameters), respectively. The LTQ-FT-ICR spectra were taken at a RP_{FWHM} at *m/z*=400 of 100,000 and an AGC target of 1.00×10^{6}. Both the LTQ-Orbitrap XL spectra in **Figure 7b** and **Figure 7c** (before and after manual adjustment of the installation parameters, respectively) were acquired at an RP_{FWHM} at *m/z*=400 of 60,000 and an AGC target of 1.00×10^{6}. The red dots above each peak in all three spectra are indicative of the theoretical peak heights for the isotopic distribution of DY 42. **Figure 7b** and **Figure 7c** display the vast difference in the results acquired before and after manual adjustment of the installation parameters. The MMA is an order of magnitude better, and the spectral accuracy is significantly better (lower χ^2 value – *vide infra*) upon parameter adjustment of the installation parameters. These data suggest that a standard molecule or procedure must be used (in addition to the tuning protocol provided by the manufacturer) to determine whether or not the instrument is performing optimally. Importantly, upon manual adjustment of the LTQ-Orbitrap XL

installation parameters, **Figure 7a** (LTQ-FT-ICR) and **Figure 7c** (LTQ-Orbitrap XL) show that the two instrument platforms are both capable of acquiring the correct results.

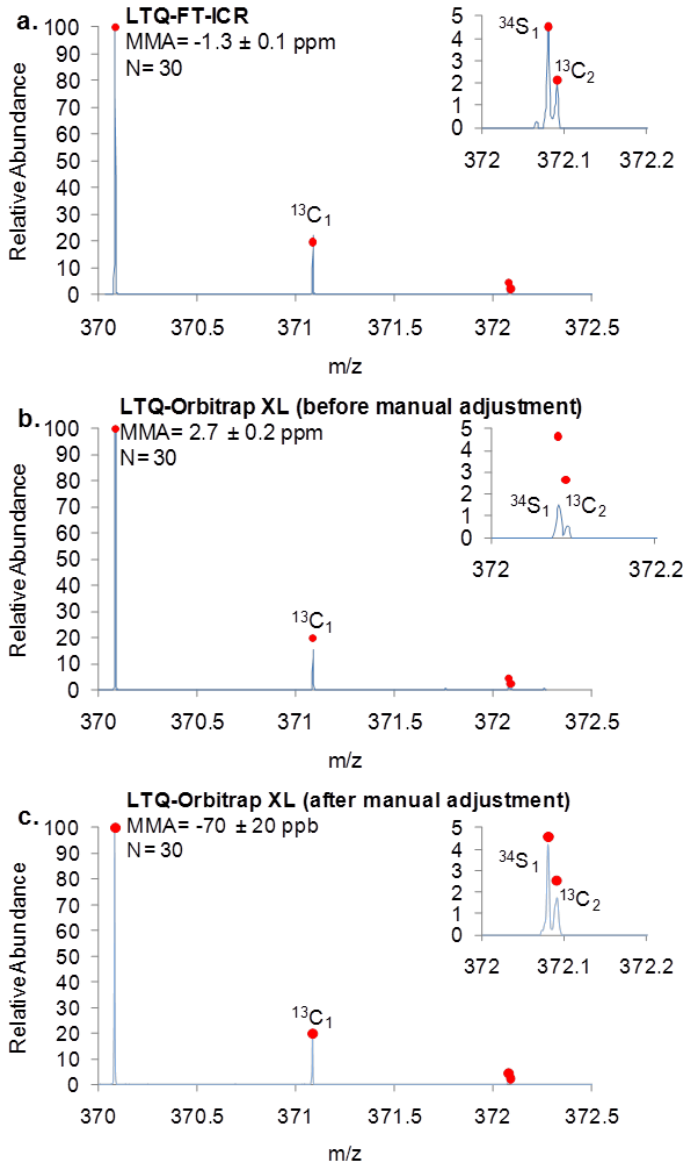

Figure 7. Single acquisition FTMS spectra of Disperse Yellow 42 dye: a) spectrum acquired on 7 Tesla LTQ-FT-ICR mass spectrometer at AGC 1.00×10^6 and RP_{FWHM} 100,000 at *m/z*=400, b) spectrum acquired on LTQ-Orbitrap XL at AGC of 1.00×10^6 and RP_{FWHM} 60,000 at *m/z*=400 before manual adjustment, and c) spectrum acquired on the LTQ-Orbitrap XL at AGC of 1.00×10^6 and RP_{FWHM} 60,000 at *m/z*=400 after manual adjustment.

3.2.1 Mass Measurement Accuracy

Plots of the MMA of the monoisotopic peak of each spectrum and the average MMA with 95% confidence intervals at each resolving power are shown for the LTQ-FT-ICR and LTQ-Orbitrap XL (after installation parameter adjustment) in **Figure 8**. **Figure 8a and Figure 8c** are shown at an AGC target of 5.00×10^5 and **Figure 8b** and **Figure 8d** are shown at an AGC target of 1.00×10^6. The oleamide ion (*m/z* 282.2791) was used for lock-mass during the LTQ-Orbitrap XL analysis. Lock-mass is an internal *m/z* standard used to correct for fluctuations due to temperature and high voltages *(96, 118)* and can allow for sub-ppm MMA.

Spectra acquired on the LTQ-FT-ICR produced MMA below 2 ppm for AGC targets 5.00×10^5 and 1.00×10^6. The average MMA ± 95% confidence interval of 30 spectra produced by the LTQ-FT-ICR at AGC target 1.00×10^6 and RP_{FWHM} 100,000 was -1.3 ± 0.1 ppm (Figure 8a). The average MMA ± 95% confidence interval of 30 spectra produced on the LTQ-Orbitrap XL, before adjustment of the installation parameters, at AGC target 1.00×10^6 and RP_{FWHM} 60,000 was 2.7 ± 0.2 ppm (**Figure 8b**). After the installation parameter optimization on the LTQ-Orbitrap XL, the average MMA ± 95% confidence interval of 30 spectra at AGC target 1.00×10^6 and RP_{FWHM} 60,000 was -70 ± 20 ppb (**Figure** 7**c**). Upon correction of the LTQ-Orbitrap XL, both instruments performed within manufacturers specifications; however, with lock-mass enabled the LTQ-Orbitrap XL is capable of ppb mass accuracy. A consistent positive bias and MMA values routinely greater than 2.5 ppm were observed in the LTQ-Orbitrap XL data before parameter optimization (data not shown) at all resolving powers for AGC targets 5.00×10^5 and 1.00×10^6. After the

parameters mentioned above were adjusted on the LTQ-Orbitrap XL, the data quality improved significantly with MMA values routinely less than 1 ppm.

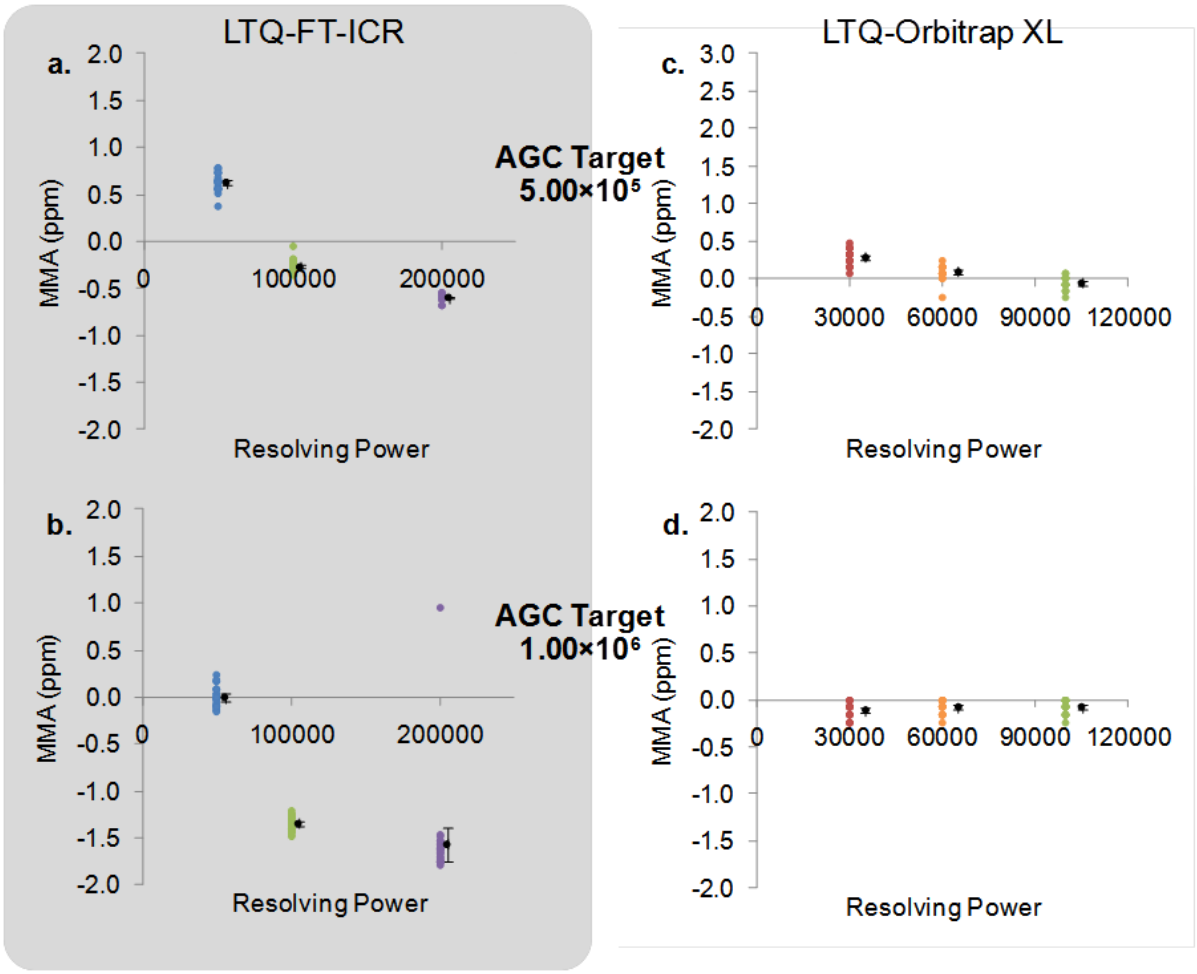

Figure 8. The calculated MMA of the monoisotopic peak for the LTQ-FT-ICR data (**a** and **b**) and the LTQ-Orbitrap XL data after manual adjustment (**c** and **d**) are plotted against the RPFWHM at m/z = 400. The series in black indicates the averages and the 95% confidence intervals of the measurement (N=30). The data points next to each averaged point are the calculated MMA's for each individual spectrum acquired. The AGC target values evaluated: **a** and **c)** 5.00×10^5 and **b** and **d)** 1.00×10^6.

3.2.2 Spectral Accuracy and Sulfur Counting

The χ^2 value of the isotopic distribution was used to "quantify" spectral accuracy in these experiments; a high χ^2 value is indicative of poor spectral accuracy. The calculated χ^2 values as a function of resolving power can be seen in **Figure 9** at AGC targets of 5.00×10^5 (**Figure 9a** and **Figure 9c**) and 1.00×10^6 (**Figure 9b** and **Figure 9d**), for both the LTQ-FT-ICR (**Figure 9a** and **Figure 9b**) and the LTQ-Orbitrap XL (**Figure 9c** and **Figure 9d)** . The sulfur peak relative abundance can be seen on the left y-axis of the same plots. Spectral accuracy plots for initial data produced by the LTQ-Orbitrap XL before manual adjustment (data not shown) suggest a decrease in spectral accuracy as the resolving power increased, agreeing with the findings of Erve *et al. (100)*; however, this correlation was not observed after the instrument parameters were changed on the Orbitrap or in any of the data collected on the LTQ-FT-ICR. After optimization of the mentioned installation parameters, spectral accuracy in the LTQ-Orbitrap XL improved by 84.4%.

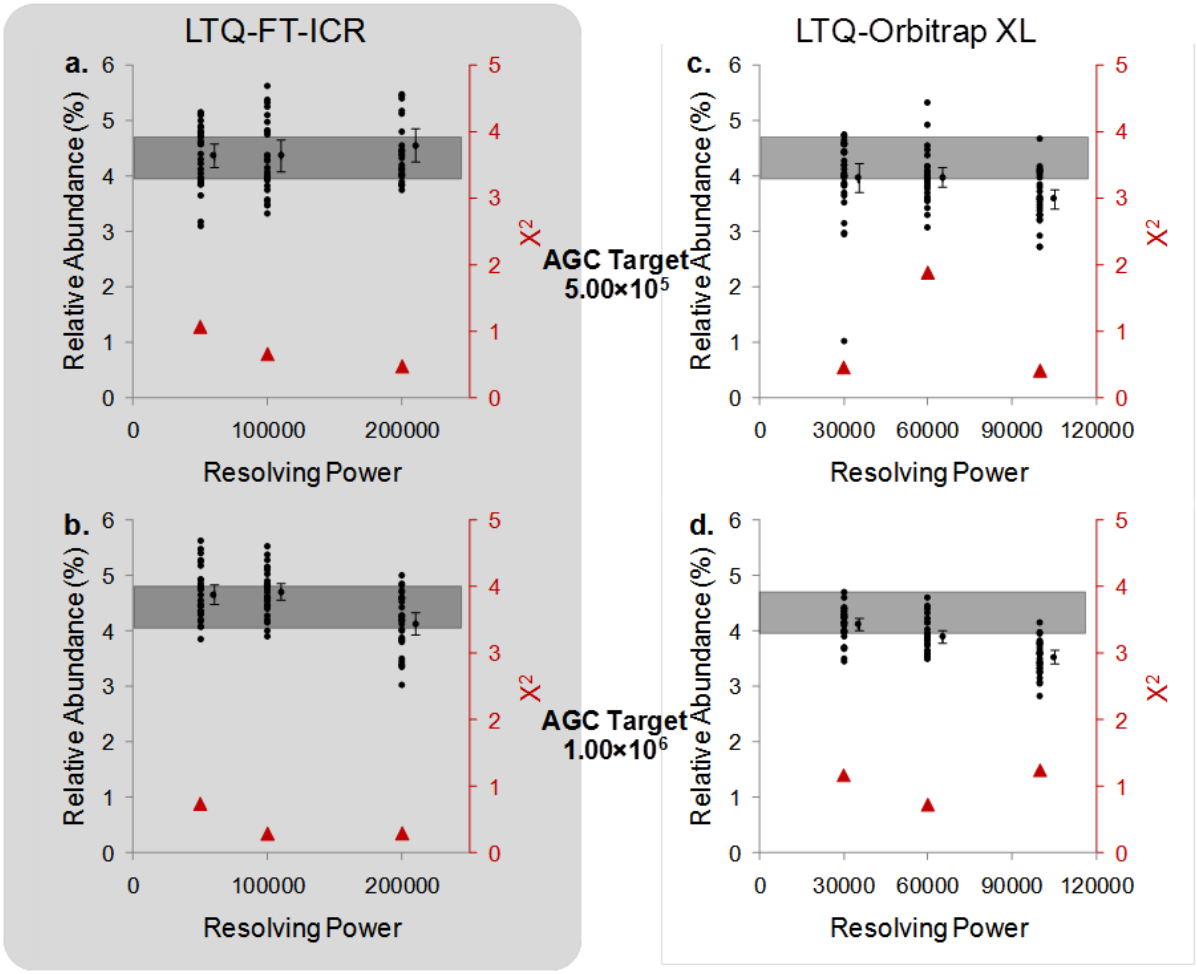

Figure 9. The relative abundance of $^{34}S_1$ to the monoistopic peak (left hand axis) for the LTQ-FT-ICR data **(a** and **b)** and the LTQ-Orbitrap XL data after manual adjustment **(c** and **d)** are plotted against the RP_{FWHM} at *m/z* = 400. The χ^2 value for the entire isotopic distribution is also plotted (right hand axis) with the red filled triangles (▲) being the calculated χ^2 value. The average sulfur peak abundance (N=30) is the black circle series with 95% confidence interval error bars. The points next to each averaged point are the sulfur peak abundances for each individual spectrum. The gray bar indicates the range of natural variation of the ^{34}S isotope as reported by NIST, 3.976%-4.734% *(103)*. The AGC target values evaluated: **a** and **c)** 5.00×10^5 and **b** and **d)** 1.00×10^6.

Erve et al. noted that spectral accuracy decreased as resolving power increased; they attributed this to isotopic beating *(100, 119, 120)*. However, the closer two frequencies are the longer the beat period, meaning the specific isotopes interact less during the measurement period. Moreover, in their work, the isotopic fine structure was unresolved; in large part due

to the fact the compounds they studied had a significantly higher *m/z* (lower frequency) than this study. In this study, we were able to resolve the $^{13}C_2$ from the $^{34}S_1$ isotopic peaks and thus, determine their individual frequencies in both the LTQ-FT-ICR and the LTQ Orbitrap XL using the diagnostic mode. The isotopic beat periods for this doublet were 0.116 and 0.196 seconds in the LTQ-FT-ICR and LTQ-Orbitrap XL, respectively, which is small relative to the measurement period (~1 second) for a typical analysis. In contrast the beat period for the monoisotopic peak and the A+1 peak in the LTQ-FT-ICR and LTQ-Orbitrap XL were ~0.0013 and ~0.002 seconds, respectively. While the beat period is much longer for the A+2 doublets relative to the ^{13}C isotopes (a factor of ~90 for the LTQ-FT-ICR and 149 for the LTQ-Orbitrap) this should be sufficient to provide high spectral accuracy for the entire isotopic distribution. This is consistent with our findings. Thus, we attribute the findings of Erve *(100)*, consistent with our LTQ-Orbitrap findings before manual optimization, to be their instrument settings rather than being related to isotopic beat patterns. We are currently pursuing these incongruent observations with more detailed studies.

The sulfur peak relative abundances produced by the LTQ-FT-ICR were within the expected natural abundance range for one sulfur atom at all resolving powers studied for AGC targets 5.00×10^5 and 1.00×10^6, demonstrating the capability of the LTQ-FT-ICR to accurately resolve the $^{34}S_1$ and $^{13}C_2$ peaks and quantify the number of sulfurs.

Analysis of the A+2 peak of the spectrum for the LTQ-Orbitrap XL data acquired before manual adjustment showed peak heights (≤3% relative abundance) systematically lower than the theoretical abundance which did not give an accurate indication of the number of sulfur atoms in the compound (data not shown); however, the A+2 peak heights for the

data taken after the LTQ- installation parameters were changed are within the expected peak height range for a compound containing one sulfur. The average sulfur peak height ± 95% confidence interval for the LTQ-Orbitrap XL at AGC target 1.00×10^6 and RP_{FWHM} 60,000 before the parameter optimization was 1.82 ± 0.11, compared to 3.91 ± 0.21 after parameter optimization.

3.3 Conclusions

The small molecule analysis capabilities in the context of MMA, spectral accuracy, and sulfur counting were compared for the LTQ-FT-ICR and the LTQ-Orbitrap XL. Both instruments were reported by Thermo Fisher Scientific to be performing at manufacturer specifications, but initially the LTQ-Orbitrap XL was far outperformed by the LTQ-FT-ICR. A more in depth inspection of the Orbitrap XL installation parameters, outside of the user tuning procedure, yielded significantly improved data. Sulfur counting was successful using the LTQ-FT-ICR and LTQ-Orbitrap XL platforms at AGC targets 5.00×10^5 and 1.00×10^6. Based on these results, the LTQ-Orbitrap XL is a suitable replacement technology for the LTQ-FT-ICR for small molecule sulfur counting and isotopic distribution analysis to yield more confident elemental composition assignments.

Due to the LTQ-Orbitrap XL passing all manufacturer tuning procedures, yet still acquiring data with ≥2.5 ppm MMA in the experiments before the manual adjustment, the authors suggest that further inspection may be needed to manually and regularly asses the performance of the LTQ Orbitrap XL. A simple assessment of performance is spectral accuracy analysis of the LTQ-Orbitrap calibration mix. This mix includes MRFA (Met-Arg-

Phe-Ala peptide, m/z 524), which contains one sulfur atom. Thus, the height of the resolved 34S peak in the A+2 peak of the normalized MRFA isotopic distribution should be within the natural abundance levels of ^{34}S and can be used to determine if the instrument is out of specification and whether adjustment of the parameters mentioned needs to be considered. Specifically, the average relative intensity of the A+2 peak measured in SIM or MS_2 mode (centered on *m/z* 524 with isolation width of at least 10 Da, AGC target 1.00×10^5 in either mode and 0 collision energy, first *m/z* 150 for MS_2 mode) should not be lower than 3% for resolving power settings 60,000 and 100,000 *(118)* (preferably, it should be around 4%). This will allow for facile and routine assessment of the LTQ-Orbitrap XL performance in order to assure the highest possible quality of data is acquired *(121).*

Chapter 4. A Liquid Chromatography Mass Spectrometry Approach using Advanced Statistics for Comparative Finished Fiber Characterization

In Chapter 4, the construction of a model database containing fifty known acid dyes is discussed. In addition to the database, ten unknowns, which include five from the database and five outside the database to account for false positives, were tested to establish a proof of concept that the database could be expanded and statistically validated. The Agilent Qualitative Analysis B.04 software correctly identified the unknown dyes; however, the software cannot be used with other data types and only considers retention time and accurate mass as descriptors. Other statistical identification methods were investigated to enhance the availability and usability across different laboratories. k-NN classification after data pretreatment by PCA analysis was used to investigation the discriminating capability of

descriptors, such as peak efficiency (N), capacity factor, *m/z*, z, the relative abundance of the M+1 peak, and the relative abundance of the M+2 peak from LC-MS data for unknown identification.

4.1 Experimental

4.1.1 Sample Preparation

Fifty acid dye samples, **Table 1**, from various manufacturers were used in the construction of the database. The samples were chosen from dyes known to be used in the textile dyeing industry, and were used without prior purification. The commercial dye powders were dissolved in the starting mobile phase of the HPLC gradient at a concentration of 1 mg/mL then diluted to a concentration of 30 µg/mL. Each sample was spiked with 10 µg/mL uracil (SIGMA-Aldrich, St Louis, MO). All samples were filtered before analysis using a 0.2 µm PVDF filter (Whatman).

Table 1. Fifty dyes included in the mini-database.

C.I Number	C.I. Name	Manufacturer	Trade Name	Chemical Formula	Monoisotopic Neutral Mass
15510	Acid Orange 7	Fisher Scientific Co.	Orange II (88%)	$C_{16}H_{12}N_2O_4S$	328.0518
15970	Acid Orange 12	Aldrich Chemical Co.	Crocein Orange G (FW 350.33)	$C_{16}H_{12}N_2O_4S$	328.0518
45350	Acid Yellow 73	Sigma	Fluorescein (FW 332.3)	$C_{20}H_{12}O_5$	332.0685
13065	Acid Yellow 36	Ciba-Geigy	Erio Metanil Yellow II	$C_{16}H_{15}N_3O_3S$	353.0834
56205	Acid Yellow 1	Crompton & Knowles	Intracid Flavine B	$C_{19}H_{14}N_2O_5S$	382.0623
62055	Acid Blue 25	M. Dohmen	Dorasyn Blue AG	$C_{20}H_{14}N_2O_5S$	394.0623
62045	Acid Blue 62	ICI Americas Inc.	Nylomine Blue A-2P	$C_{20}H_{20}N_2O_5S$	400.1093
17102	Acid Red 337	Clariant	Nylosan Red E/C2GN P 200	$C_{17}H_{12}N_3O_4SF_3$	411.0501
61530	Acid Blue 27	Ciba-Geigy	Eriosin Blue 3G	$C_{22}H_{18}N_2O_5S$	422.0936
17200	Acid Red 33*	D&C	Red 33 (85%)	$C_{16}H_{13}N_3O_7S_2$	423.0195
18640	Acid Yellow 49	Mobay Chemical Co.	Telon Yellow FGL 200	$C_{16}H_{13}N_5O_3SCl_2$	425.0116
14205	Acid Yellow 199	M. Dohmen	Dorasyn Yellow A3R 200%	$C_{19}H_{16}N_4O_6S$	428.0791
63010	Acid Blue 45*	Ciba Geigy	Erio Cyanine S 150%	$C_{14}H_{10}N_2O_{10}S_2$	429.9777
26660	Acid Red 116	DyStar	Telon Red 2BN	$C_{22}H_{16}N_4O_4S$	432.0892
26900	Acid Red 151	Marlowe-Van Loan Sales Co.	Marvanyl Red HCO	$C_{22}H_{16}N_4O_4S$	432.0892
62058	Acid Blue 129	Sandoz Chemical	Nylosan Blue P-RL	$C_{23}H_{20}N_2O_5S$	436.1093
26501	Acid Orange 156	Ciba Geigy	Tectilon Orange 3G200	$C_{21}H_{20}N_4O_5S$	440.1154
17101	Acid Red 266	M. Dohmen	Dorasyn Red A-2B 200%	$C_{17}H_{11}N_3O_4SF_3Cl$	445.0111
62125	Acid Blue 40	M. Dohmen	Dorasyn Blue A2G 200 %	$C_{22}H_{17}N_3O_6S$	451.0838
26502	Acid Orange 127	Sandoz Chemical	Nylosan Orange N-RL	$C_{24}H_{20}N_4O_4S$	460.1205
17045	Acid Red 37*	Aldrich Chemical Co.	AR37 (524.44)	$C_{18}H_{16}N_4O_8S_2$	480.0410
18965	Acid Yellow 17*	Sandoz Chemical	Sandolan Yellow E-2GL	$C_{16}H_{12}N_4O_7S_2Cl_2$	505.9524
11714	Acid Yellow 220	Ciba Specialty Chemical	Lanaset Yellow 2R	$C_{23}H_{19}N_4O_7SCl$	530.0663
16185	Acid Red 27	DyStar	Isolan Scarlet K-GLS gran 150%	$C_{20}H_{14}N_2O_{10}S_3$	537.9811
44025	Acid Green 16	Ciba Geigy	Erio Green B Conc.	$C_{27}H_{27}N_2O_6S_2$	538.1232
61203	Acid Blue 227	Ciba Geigy	Tectilon Blue 4R	$C_{24}H_{23}N_3O_8S_2$	545.0927
45100	Acid Red 52	Ciba Geigy	Erio Red XB	$C_{27}H_{30}N_2O_7S_2$	559.1573
14170	Acid Yellow 65	Ciba-Geigy	Erio Jasmine G	$C_{25}H_{20}N_4O_8S_2$	568.0723
20470	Acid Black 1*	Atlantic	Acid Black 10BR crude	$C_{22}H_{16}N_6O_9S_2$	572.0420

Table 1. Continued

C.I. Number	C.I. Name	Manufacturer	Trade Name	Chemical Formula	Mass
14172	Acid Orange 67-1	Huntsman	Erionyl Yellow A-R-01	$C_{26}H_{22}N_4O_8S_2$	582.0879
13390	Acid Blue 92*	D&G Dyes	Doracid Blue RL	$C_{26}H_{19}N_3O_{10}S_3$	629.0233
61585	Acid Blue 80*	Sandoz Chemical	Nylosan Blue F-L	$C_{32}H_{30}N_2O_8S_2$	634.1444
26360	Acid Blue 113*	Sandoz Chemical	Nylosan Navy N-RBL	$C_{32}H_{23}N_5O_6S_2$	637.1090
50320	Acid Blue 102	Mobay Chemical Co.	Telon Fast Blue GL 200	$C_{35}H_{26}N_4O_7S_2$	678.1243
22910	Acid Yellow 42*	D&G Dyes	Doracid Yellow R 200%	$C_{32}H_{26}N_8O_8S_2$	714.1315
20530	Acid Red 158*	Miles	Telon Red ERNA	$C_{32}H_{22}N_5O_{10}S_3$	733.0607
23266	Acid Red 111*	Sandoz Chemical	Nylosan Scarlet F-3GL	$C_{37}H_{30}N_4O_{10}S_3$	786.1124
23635	Acid Red 114*	Ciba Geigy	Erionyl Red RS	$C_{37}H_{30}N_4O_{10}S_3$	786.1124
18732	Acid Orange 60	Ciba Geigy	Irgalan Orange 2RL200	$C_{32}H_{26}CrN_{10}O_8S_2$	794.0782
42660	Acid Blue 83*	Sandoz Chemical	Sandolan Syanine N6B	$C_{45}H_{45}N_3O_7S_2$	803.2699
13906	Acid Yellow 151	M. Dohmen	Dorolan Yellow RTU	$C_{32}H_{28}CoN_8O_{10}S_2$	807.0702
24125	Acid Red 128*	Sandoz Chemical	Nylosan F-BRN	$C_{37}H_{30}N_4O_{12}S_3$	818.1022
42655	Acid Blue 90*	Sandoz Chemical	Sandolan Cyanine N-G	$C_{47}H_{49}N_3O_7S_2$	831.3012
15707	Acid Blue 193	BASF	Acidol Dark Blue M-TR	$C_{40}H_{24}CrN_4O_{10}S_2$	836.0339
12230	Acid Black 58	Ciba-Geigy	Irgalan Grey BL KWL 200	$C_{38}H_{30}CrN_6O_{10}S_2$	846.0870
18165	Acid Black 60	DyStar	Isolan Grey KPBL200	$C_{38}H_{32}CrN_8O_{10}S_2$	876.1088
13900	Acid Yellow 99	Sandoz Chemical	Vitrolan Yellow GR	$C_{32}H_{24}CrN_8O_{16}S_2$	892.0157
15711	Acid Black 172	Ciba Specialty Chemical	Lanaset Black B	$C_{40}H_{22}CrN_6O_{14}S_2$	926.0040
14880	Acid Blue 158	Ciba-Geigy	Neolan Blue 2G	$C_{40}H_{24}CrN_4O_{16}S_4$	995.9475
18810	Acid Red 186	BASF	Palatin Fast Pink BNI	$C_{40}H_{28}CrN_8O_{16}S_4$	1055.991

4.1.2 Analysis via HPLC-Q-TOF

The samples were analyzed via a 1200 Series Agilent HPLC coupled to an Agilent 6520 Accurate-Mass Q-TOF (Agilent Technologies, Santa Clara, CA) with internal calibration per manufacturer specifications. Mobile phase A and B consisted of 20 mM ammonium formate adjusted to pH 4 with formic acid and 70:30 methanol:acetonitrile, respectively. The solvents (Burdick and Jackson, Muskegon, MI) and the ammonium

formate (SIGMA-Aldrich, St Louis, MO) were HPLC grade and the formic acid (SIGMA-Aldrich, St Louis, MO) was MS-grade. The mobile phases were filtered using a vacuum filtration apparatus (**Figure 10**) with a Millapore Durapore 0.22 µm PVDF membrane filter. The column used for analysis was a Zorbax Eclipse Plus C_{18} (2.1×50 mm, 3.5 µm) with a Zorbax Eclipse Plus C_{18} narrow bore guard column (2.1×12.5 µm, 5 µm). The following gradient was applied at a flow-rate of 0.25 mL/min: 5% B (0-2 min), 5-90% B (2-9 min), 90% B (9-19 min), 90-5% B (19-19.5 min) with a 6-min post-time between runs at 5% B. The samples were run in triplicate with a solvent blank between each sample.

The mass spectrometer was equipped with a dual electrospray ionization source in negative ionization mode. The fragmentor and capillary voltages were 110 and 4000 V, respectively. The drying gas temperature was 350°C. The instrument was tuned and calibrated before analysis per the manufacturer specifications.

Figure 10. Vacuum filtration set-up for HPLC-MS solvent preparation.

4.1.3 Data Analysis

Data analysis was completed using Agilent Qualitative Analysis B.04 software as well as Matlab Ver. 7.10.0.499 and JMP® Pro 9.0.0. The Agilent Qualitative Analysis software uses a spreadsheet containing the accurate mass, retention time, and chemical formula of the compounds. The list was used to identify the unknowns with a specified retention time window of 0.1 minute and a 5-ppm mass window. If a chemical formula for the compound is present on the spreadsheet, the score generated by the software also includes the overall fit of the isotopic distribution, abundance and spacing, of the suspected formula. If no formula is present the software only considers mass and retention time.

Other statistical approaches were investigated expanding the data characteristics investigated, such as capacity factor. PCA was used with either the k-NN method or the K-means cluster algorithm to identify the unknown dyes in pattern space. PCA was used to arrange the known dyes in pattern space with *n* number of dimensions (where *n* equals the number of descriptors). k-NN analysis in Matlab® was used to match each unknown to its closest neighbor using its Euclidean distance. An arbitrary distance of 5 was determined to be the cutoff for a false positive identification. In the JMP® software, the K-means clustering method was used to identify the unknowns. A standard deviation in the masses of the dyes in the cluster greater than 1.00 was used to determine whether the classification was correct. In these experiments, the descriptors studied were capacity factor, *m/z*, z, accurate mass, and the relative isotopic abundances of the M+1 and the M+2 peaks.

Equation 7 shows the equation for capacity factor, k', where t_M is instrument dead time. Capacity factor was used in lieu retention time to allow for the use of the database by

different labs when the same method (including gradient, stationary phase, and mobile phases) is employed *(84)*. Uracil, because it is not retained on a reverse phase column, was spiked into the samples and used for the determination of the dead time of the instrument.

Equation 7. Capacity factor

$$k' = \frac{t_R - t_M}{t_M}$$

4.2 Results and Discussion

There are 59 dye structural components in the 50 dyes studied. C.I. Acid Black 172 contained five colored components, C.I. Acid Blue 158 contained two colored components, and C.I. Acid Orange 127 contained two colored components. The unknowns used did not contain multiple component dyes; however, there were instances of both singly and doubly charged species of the same ion present depending on the number of sulfonic acid groups found in the structure. **Table 1** shows a complete list of the dyes studied. Shown in **Figure 11** are three of the dyes studied, each with a different representative chromophore (shown in red). **Figure 11a** shows C.I. Acid Blue 113 with two azo chromophores shown in red, as well as two sulfonic groups producing both $[M\text{-}H^+]^{1-}$ and $[M\text{-}2H^+]^{2-}$ at *m/z* 636.1000 and *m/z* 317.5468, respectively, in the corresponding spectrum. **Figure 11b** shows C.I. Acid Blue 25 with an anthraquinone chromophore shown in red with the $[M\text{-}H^+]^{1-}$ ion at *m/z* 393.0549, shown in the corresponding spectrum. **Figure 11c** shows C.I. Acid Green 16 with the triphenylmethane chromophore highlighted in red producing an $[M\text{-}H^+]^{1-}$ of *m/z* 593.1774 in the corresponding spectrum.

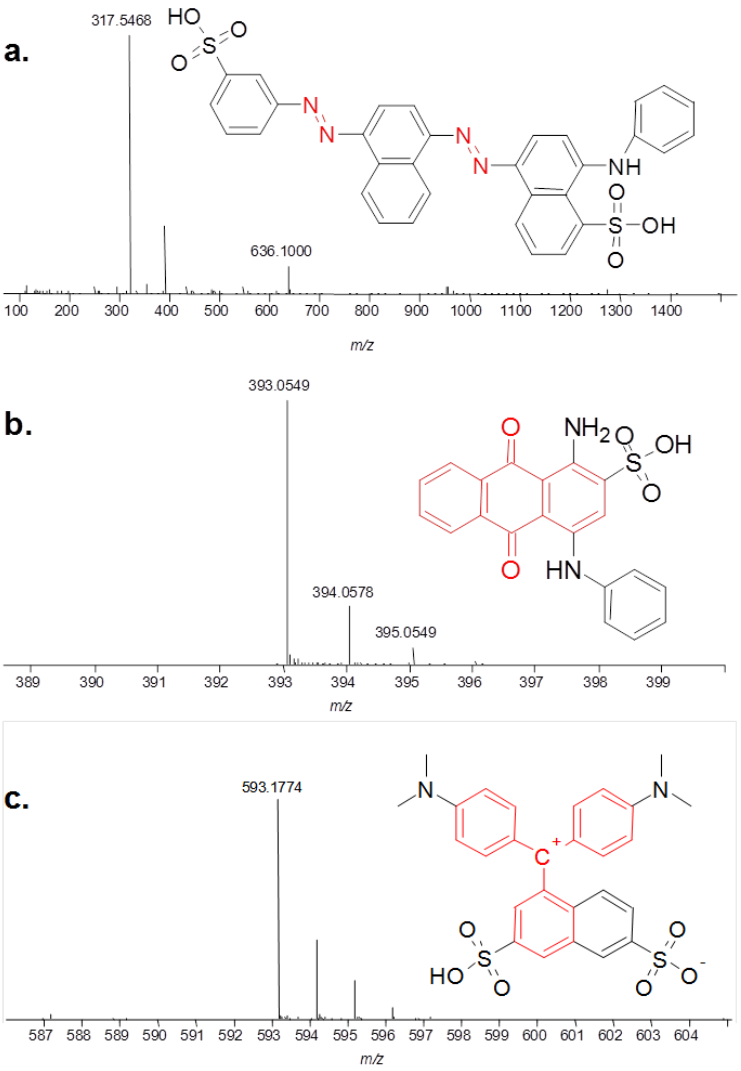

Figure 11. Dye structures and their corresponding spectra containing for three of the dyes used in the construction of the database with examples of the three chromophore most commonly found in acid dyes; **a)** C.I. Acid Blue 113 containing two azo groups (shown in red) as well as two sulfonic acid groups resulting in both $[M-H]^{1-}$ and $[M-2H]^{2-}$ in the spectrum, *m/z* 636.1000 and *m/z* 317.5468, respectively; **b)** C.I. Acid Blue 25 containing an anthraquinone chromophore (shown in red) and characteristic spectrum with $[M-H]^{1-}$ at *m/z* 393.1549; and **c)** C.I. Acid Green 16 containing a triphenylmethane functional group (shown in red) and characteristic spectrum with a molecular ion of $[M-H]^{1-}$ at *m/z* 593.1774.

Using the Agilent Qualitative Analysis B.04 software, the unknown dyes were correctly identified and the five unknowns introduced to account for the possibility of false positives were unable to be identified as a dye present in the database. The results for the

identification of the unknowns using the Agilent software are summarized in **Table 2**. The software was unable to generate chemical formulas for unknowns 6, 7, and 9 but was able to correctly identify the unknowns that were present in the database within the set parameters. The software searches a list of known dye masses and retention times within a specified mass and retention time window. The software is sensitive to the dye order in the database and will choose the first dye it comes across with the correct mass and retention time within the specified windows which could be problematic in the case of isomer dyes.

Table 2. Results of the database search using the Agilent B.04 Qualitative Analysis software.

Unknown	Name	Formula	Score	Mass	Reference Mass	t_R	t_R Diff (min)	Mass Diff (ppm)
10	ABLK1	C22 H16 N6 O9 S2	94.89	572.0428	572.0416	12.701	0.022	-2.08
9	AG16	C31 H34 N2 O6 S2	99.3	594.1856	594.1852	12.221	0.011	-0.75
8	AY220		96.3	693.1279	693.129	15.27	-0.122	1.65
7	AR27		75.32	851.1464	851.15	15.183	0.001	4.23
6	ABLK60		85.31	847.0871	847.0898	13.411	0.006	3.17

The scores shown in **Table 2** are a score out of 100 calculated by an algorithm, **Equation 8,** which is based on how well the measured mass, isotope abundances, isotope spacing, and retention time fit what would be expected of the database entry. If the database entry for a given dye only consists of mass and retention time then the formula does not consider isotopic spacing and abundances. The factors mentioned are used to calculate match probabilities, **Equation 9**, where x is the difference between the expected value from the database entry and the measured values and σ is a program assigned value for the expected data variation. The weights are a set of values set by the Agilent software that are

based on 600 different samples and were chosen to achieve optimum results. The mass weight ($W_{mass)}$ is 100, abundance weight ($W_{abundance)}$ is 60, spacing weight ($W_{spacing}$) is 50, and retention time weight (W_{RT}) is 100.

Equation 8. Overall score for the comparison of the database compound and the unknown compound.

$$Score = \frac{(W_{mass} \times P_{mass} + W_{abundance} \times P_{abundance} + W_{spacing} \times P_{spacing} + W_{RT} \times P_{RT})}{W_{mass} + W_{abundance} + W_{spacing} + W_{RT}}$$

Equation 9. Match probability between the database values and the experimental values for mass, isotopic spacing, isotopic abundances, and retention time.

$$P = e^{x^2/\sigma^2}$$

4.2.3 Statistical Analysis

Multiple descriptors were considered to determine the most useful data to be included in a forensic LC-MS dye database. The use of mass versus mass and charge as separate entities in the statistical model was made. When separately considering *m/z* and z, there is a possibility of multiple entries for a single compound, due to the presence of both singly and doubly charged ions, complicating the data set. Using mass allows for the data set to be simplified and ensures that there are no redundancies. Another descriptor that was considered was N (peak efficiency) as a measure of peak shape. N did not help in the discrimination of the dyes and ultimately added to possible errors in the data due to the large variation in the calculation within triplicate runs.

4.2.2.1 k-Nearest Neighbor

k-NN analysis was used to calculate the distance between an unknowns and the closest known database dye in pattern space after data pretreatment by PCA. **Figure 12** shows the plot generated by the k-NN program created using Matlab® to identify the unknown dyes. Unknown 9, shown in red, was inserted into pattern space alongside the known dyes to aid in visualization of the classification. The program matched all of the unknowns to a potential dye using the cityblock distance between the unknown and the closest point in pattern space. An arbitrary cityblock distance of 5 was used as the cut-off for an incorrect identification; this was the case for unknowns 1 through 5, which ranged in city block distance in pattern space from 5 to 20. The unknowns that were correctly matched to the dyes in the database where unknown 6 with a distance of 0.347 from Acid Black 60, unknown 7 with a distance of 1.537 from Acid Red 27, unknown 8 with a distance of 0.587 from Acid Yellow 220, unknown 9 with a distance of 2.538 from Acid Green 16, and unknown 10 with a distance from Acid Black 1 of 1.428.

The analysis of unknowns using the k-NN algorithm, correctly identified all the unknowns present in the 50 dye reference set. Capacity factor, mass, M+1 peak height, and M+2 peak height were used as descriptors for this data analysis method. Increasing the arbitrary city block distance cutoff to a value greater than 5 would result in unknown 1 being misidentified as Acid Yellow 99 regardless of a mass difference of 3 Da between the two dyes. The greatest distance from an unknown to its database counterpart was 2.538 between unknown 8 and Acid Green 16.

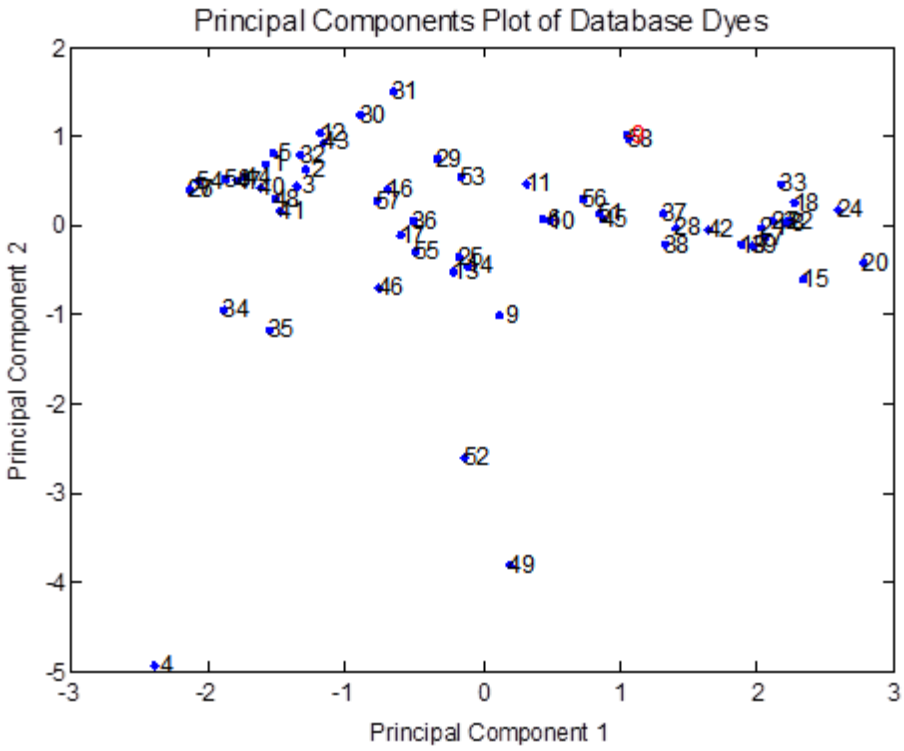

Figure 12. Results of the k-NN analysis using Matlab® software. All 59 data points describing the 50 dyes are shown with unknown 9 inserted into pattern space, shown in red. The descriptors used for the k-NN analysis were k', mass, M+1, and M+2 isotopic abundances.

4.2.2.2 k-means Cluster Analysis

Another method that was considered was k-Means cluster analysis after data pretreatment with PCA. **Figure 13** shows the summary plots of the PCA of acid dye data generated by the JMP® software. The summary plot consists of the Eigenvalues generated and a bar graph of the percent of variance encompassed by each principle component. The score plot, shown in the middle, is a summary of the relationship of the dyes plotted against the first and second principle components. The loadings plot, shown on the right is a graphical representation of the relationship between the descriptors used for analysis. The factors considered for were: capacity factor, mass, M+1 peak relative isotopic abundance,

and M+2 peak relative isotopic abundance. The first and second principle components encompass 58.5% and 26% of the variance in the data set, respectively. The greater the variance encompassed by the first two principal components the greater the separation of the points in pattern space. Each point in pattern space produced by the known dyes is considered as a separate cluster and maximum separation of the points increases the distance between different dyes and causing the correct unknown/known dye cluster to be more obvious.

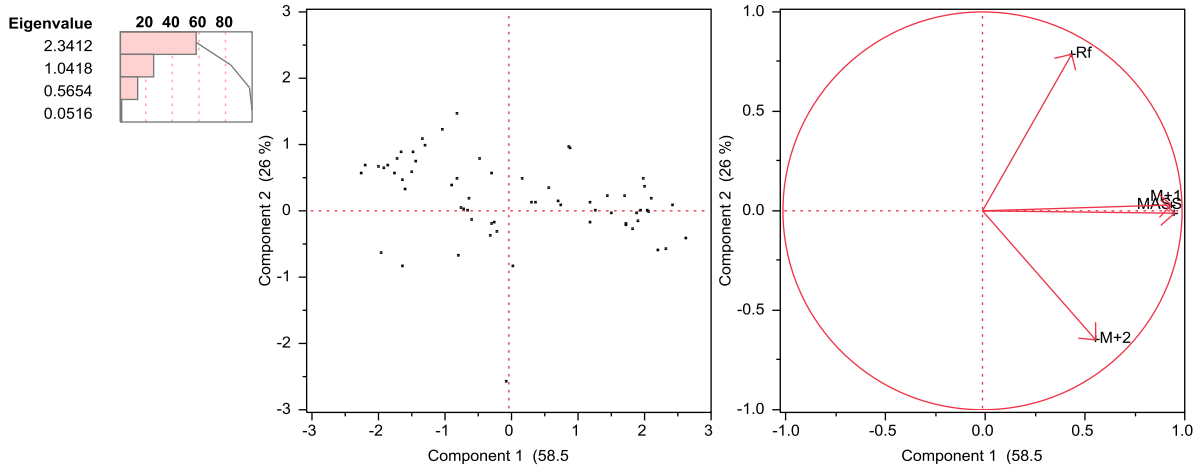

Figure 13. Summary plot for PCA of database dyes. Plots shown are Eigenvalues with percent variance (left), score plot (middle), and loadings plot (right).

The unknowns clustered with their respective known dyes found in the database using K-means are shown in **Figure 14**. The colored points inside each circle indicate the unknown dye and its database match. Each dye was correctly identified with all the dyes present in the database; however, to aid visualization of the matches the other points were removed.

Comparison of the use a mass and of *m/z* and z as separate descriptors in the database showed a greater error in classifications due to the possibility of having multiple entries for the same dye component. Considering *m/z* and z separately would be important in the case of two or more dyes with the same accurate mass but with variation in the number of sulfonic acid groups causing a difference in charge; however, this was not the case in the group of dyes studied.

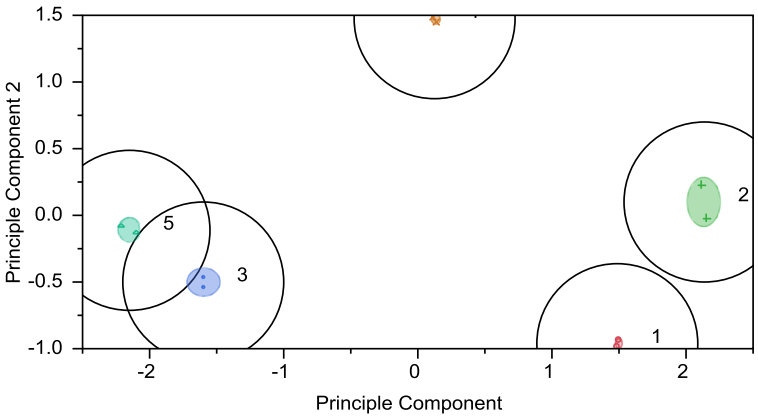

Figure 14. Unknowns with their respective database matches plotted against the first two priciple components.

A cut-off of 1.00 in the standard deviation of mass of a cluster was used to determine whether an unknown was correctly grouped to a known dye. The standard deviations of the masses of the clusters of the correctly identified dyes were all less than 0.002, which is expected given the 2 ppm mass accuracy of the Agilent 6520 Accurate Mass Q-TOF. The dyes that were not correctly identified showed standard deviations in the mass of the cluster all greater than 1.00.

Peak efficiency was used as a measurement of chromatographic peak shape. Although the unknowns were correctly identified with and without the use of column

efficiency as a descriptor, the calculation of efficiency was not reproducible between triplicate analyses of the same dye with the percent difference within triplicate runs being as high as 156% in the case of Acid Blue 80. The large differences in the calculations within triplicate runs arise from the lack of reproducibility of the measurement of chromatographic peak width at 10%. Small variations in this value largely affect the efficiency calculation. The use of efficiency as a descriptor also did not aid in the discrimination of the dyes and was ultimately ruled out as a useful descriptor.

4.3 Conclusion

Statistical analysis of the 10 "unknown dyes" tested against the preliminary database of 50 commercial acid dyes demonstrated proof of concept for the potential forensic utility for a comprehensive database of acid dyes. For the dyes studied and the analytical method used, PCA in conjunction with K-means clustering as well as PCA coupled to k-NN analysis successfully identified the five unknown dyes present in the database and did not identify the five unknown dyes not in the database within the set parameters. Charge state was considered as a separate descriptor from *m/z*; however, it did not enhance the discriminations and would just increase redundancies in the database. The number of descriptors adds to the certainty of the identification; however, the use of efficiency as a descriptor was not necessary and in fact lessened the separation between the dyes in pattern space. Mass, capacity factor, and M+1 and M+2 isotopic abundances were considered to be the most successful at describing the data in pattern space. This research shows the usefulness and

potential value of the addition of LC-MS and chemometric analysis to the field of trace evidence, specifically dyed fiber analysis.

Chapter 5. LC-Q-TOF Analysis of Dyes Extracted after Lightfastness Testing

In Chapter 5, the analysis of dyes extracted from fibers after lightfastness testing will be discussed. The acid dyed nylon fabrics were exposed to UV light using a fadeometer and sampled at various time points within a 40-hour period. The light exposure is used to simulate dyed fibers that have been exposed to sunlight over time. The hope is to find that after prolonged UV exposure the original dye molecule will still be present in a high enough concentration to be extracted, analyzed via LC-MS, and characterized using the compiled dye database.

5.1 Experimental

5.1.1 Acid Dyeing

Stock solutions (1 mg/mL) of commercial dye powder in water were diluted to produce a 300-mL dyebath for a 1% owf dyeing on 3.00 g nylon (Dupont, Spun Nylon 6.6, Type 200) then acidified to pH 4 using glacial acetic acid. The dye bath and fabric were placed into beakers and inserted into the Roaches Pyrotec MB2 dyeing machine with the following heating program: ramp rate of 4°C from room temperature to 100°C, then the temperature was help for 60-minutes. Upon completion of the dyeing program the samples were allowed to cool then rinsed using tap water and dried overnight. The dyes used in this

study are shown in **Table 3.** The dyes without chemical formulas and molecular masses are confidential and not listed in the Colour Index *(122)*.

Table 3. Dyes used for the photostability analysis using LC-MS.

C.I Number	C.I. Name	Manufacturer	Trade Name	Chemical Formula	Monoisoopic Neutral Mass	Chemical Class
15510	Acid Orange 7	Fisher Scientific Co.	Orange II (88%)	$C_{16}H_{12}N_2O_4S$	328.0518	Monoazo
62055	Acid Blue 25	M. Dohmen	Dorasyn Blue AG	$C_{20}H_{14}N_2O_5S$	394.0623	Anthraquinone
63010	Acid Blue 45*	Ciba Geigy	Erio Cyanine S 150%	$C_{14}H_{10}N_2O_{10}S_2$	429.9777	Anthraquinone
17101	Acid Red 266	M. Dohmen	Dorasyn Red A-2B 200%	$C_{17}H_{11}N_3O_4SF_3Cl$	445.0111	Monoazo
62125	Acid Blue 40	M. Dohmen	Dorasyn Blue A2G 200 %	$C_{22}H_{17}N_3O_6S$	451.0838	Anthraquinone
44025	Acid Green 16	Ciba Geigy	Erio Green B Conc.	$C_{27}H_{27}N_2O_6S_2$	538.1232	Triphenyl methane
61203	Acid Blue 277	Ciba Geigy	Tectilon Blue 46	$C_{24}H_{23}N_3O_8S_2$	545.0927	Anthraquinone
23266	Acid Red 111*	Sandoz Chemical	Nylosan ScarletF-3GL	$C_{37}H_{30}N_4O_{10}S_3$	786.1124	Disazo
23635	Acid Red 114*	Ciba Geigy	Erionyl Red RS	$C_{37}H_{30}N_4O_{10}S_3$	786.1124	Disazo
12230	Acid Black 58	Ciba-Geigy	Irgalan Grey BL KWL 200	$C_{38}H_{30}CrN_6O_{10}S_2$	846.087	Metalized Monoazo
18810	Acid Red 186	BASF	Palatin Fast Pink BNI	$C_{40}H_{28}CrN_8O_{16}S_4$	1055.991	Metalized Monoazo
-	Acid Red 361	M. Dohmen	Dorasyn Red AFB 200%	-	-	Monoazo
-	Acid Blue 324	M. Dohmen	Dorasyn Blue ABRT	-	-	Anthraquinone
-	Acid Yellow 219	M. Dohmen	Dorasyn Yellow C4RN	-	-	-

5.1.2 Degradation

The dyed nylon fabric was mounted on white cardstock and hung on metal holders inside the Atlas Ci3000+ Xenon Fade-Ometer, **Figure 15**. Samples were collected at 0, 5, 10, 15, 20, and 40-hours.

Figure 15. Atlas Ci3000+ Xenon Fade-Ometer used for timed photo-degradation study.

5.1.3 Dye Extraction

The dyed fiber (500 µg) was placed into a reacti-vial with lid (Thermo Scientific, Rockford, IL) with 200 µL of a 4/3 (v/v) Pyridine/water solution and heated in a heating block (Pierce Reacti-Therm) at 120°C for 30-minutes. The colorless fiber was removed and the vials were placed back in the heating block without their lids to evaporate the remaining solvent. Once the solvent evaporated, 200 µL of HPLC solvent at gradient starting conditions was added. The samples were filtered using a syringe (Henke Sass Wolf Gmblt disposable syringe, 1 mL) and 0.2 µm PVDF filter (Whatman) before analysis.

5.1.4 Analysis via HPLC-Q-TOF

The procedure detailed in Section 3.2.2 was used for analysis of these samples with the exception of a modified flow rate and gradient. The samples were analyzed using a flow rate of 0.5 mL/min with the following gradient: 3% B (0-1min), 3-60% B (1-1.5 min), 60-90% B (1.5-7 min), hold at 90% B (7-9 min), and 90-3% B (9-9.5 min) with a 4-min post-time between runs at 3% B.

5.2 Results and Discussion

Dyes that are to be exposed to UV radiation are usually synthesized with a built in photostabilizer that protects the dye and the polymer against photodegradation by preferentially absorbing the UV radiation, accepting the energy transfer from the excited polymer or dye, or quenching the effects of singlet oxygen *(123)*; however, the dyes studied did not include photostabilizers. The photostability of dyed polymers depends on four principle factors: the chemical nature of the polymer, the environment of the system, the physical nature of the dye, and the presence of stabilizers.

The dye extraction procedure was not quantitatively reproducible between runs of the same dye at different time points. To quantify the dye and see a degradation gradient across the seven time points, all dye must be extracted from the fiber and solubilized into the HPLC solution during sample preparation. During the extraction procedure, the colorless fiber is to be removed from the pyridine, water, and dye mixture in the vial; however, for many of the dyes the fiber still retained some color after an hour and the pyridine and water mixture had to be replenished during this process due to evaporation. Other problems arose when

reconstituting the extracts into mobile phase starting conditions. Some of the dyes would not completely go into solution and a thin dye coating remained on the vial, which was only removed after repeated rinses using both water and acetonitrile.

The dyes were sampled at time points of 0, 5, 10, 15, 20, and 40-hours. A control sample that was not exposed to the light source but was present in the fade-o-meter during the entire light exposure procedure was also analyzed for each dye studied. The dye was present in all of the samples at all of the time points except for C.I. Acid Green 16 at the 40-hour time point. C.I. Acid Green 16 was the only dye that was visibly lighter at the end of the photo degradation process. **Figure 16** shows the overlaid spectra of C.I. Acid Green 16 at 0-hours (blue) and 40-hours (green). The decrease in absorbance is indicative of the lightening of color attributed to the photodegradation process.

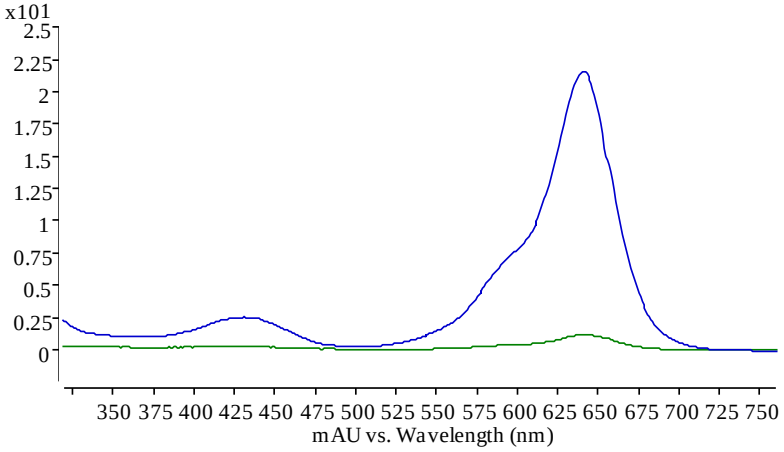

Figure 16. UV-vis spectra of C.I. Acid Green 16 at time points 0-hours (blue) and 40-hours (green).

Figure 17 shows the overlaid MS spectra of C.I. Acid Green 16 at all the time points studied, except 40-hours. The different MS spectra of each time point are represented by different colors; the control is shown in purple, 0-hours is shown in blue, 5-hours is shown in green, 10-hours is shown in black, 15-hours is shown in orange, and 20-hours is shown in red. C.I. Acid Green 16 is the only dye whose abundance decreased with increased time of exposure to light. C.I. Acid Green 16 showed the most drastic color difference between the unexposed 1% owf dyed nylon and the different time points. The fiber was almost colorless at 40-hours. C.I. Acid Green 16 contains the triphenylmethane chromophore which is known to have low lightfastness due its bulky planar structure hindering the rotation of bulky groups to dissipate the absorbed energy *(124)*.

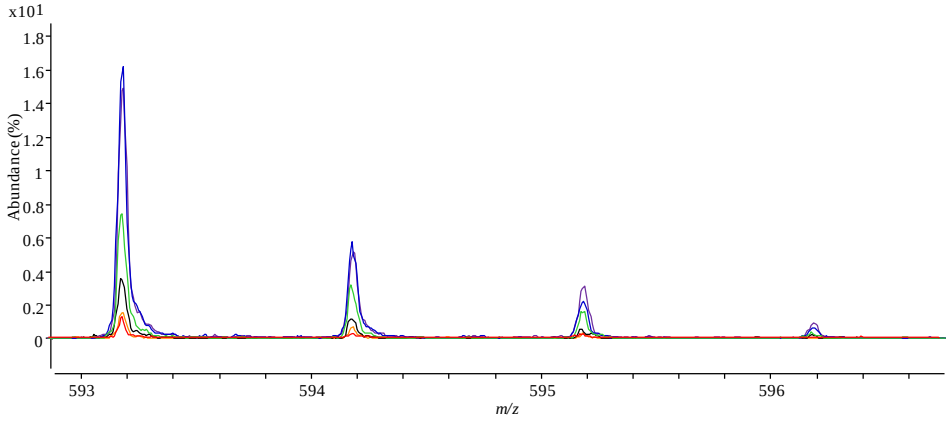

Figure 17. Isotopic distribution for C.I. Acid Green 16 over all time points, except for 40-hours.

The dye structure of C.I. Acid Red 361 is not listed in the Colour Index; however, the dye chemical class is listed as monoazo with unknown dye structure and formula. The monoisotopic mass was determined through the analyses mentioned in Chapter 4. Although

the structure of the dye is unknown, the chemical composition of the dye can be discussed. Azo dyes undergo photooxidation or photoreduction leading to fading; however, the substituents of the dye molecule can also affect fading or photostability of the azo dye. Electron withdrawing groups reduce lightfastness by pulling electrons away from the azo bond and reducing the strength of the azo link while electron donating enhance lightfastness *(124)*. A proposed structure of C.I. Acid Red 361 was found through a third-party source, the structure, shown in the inset of **Figure 18** shows the presence of electron donating groups that would lead to the enhanced light fastness of the azo dye. The overlaid spectra, **Figure 18,** show a small difference in abundance between the 0-hour time point and the 40-hour time point which cannot be attributed to the photodegradation due to the possible sample loss in the extraction procedure.

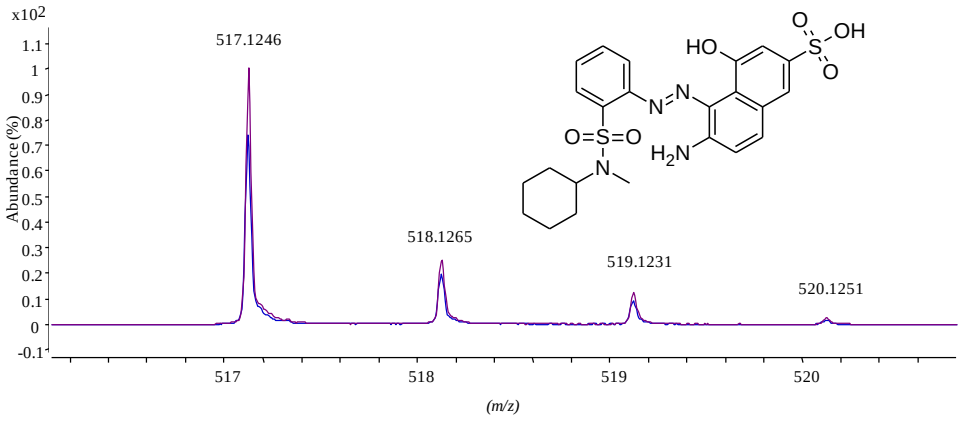

Figure 18. Overlaid MS spectra of C.I. Acid Red 361 at time points 0-hours (purple) and 40-hours (blue) with the dye structure inset.

Anthraquinone dyes are one of the most lightfast dyes depending on the nature and location of their substituents. Intramolecular hydrogen bonding with substituents in the α

position occurs. Upon absorption of light energy the dye structure is converted from a keto form to the less stable enol form that dissipates the energy through heat *(124)*. The light fastness of the dye is also dependent on the substrate, whereas, the same dye is more lightfast on polyester and less lightfast on nylon because of its strong polarity *(124)*. The hydrogen bonds in the polymer compete with the dye, reducing the light stability. Another structural component often found in anthraquinones that helps with lightfastness is the ability of the dye to dissipate energy through the rotation of bulky groups, such as phenyl groups *(124)*.

Figure 19 shows the overlaid MS spectra for 0-hours (purple) and 40-hours (blue) with the structure of C.I. Acid Blue 25 shown inset. C.I. Acid Blue 25 has an amino group α, which is typically less lightfast than a hydroxyl group *(124)*. The presence of the bulky phenyl group as well as the electron donating sulfonic acid group in the β position also contributed to the enhanced light fastness of C.I. Acid Blue 25.

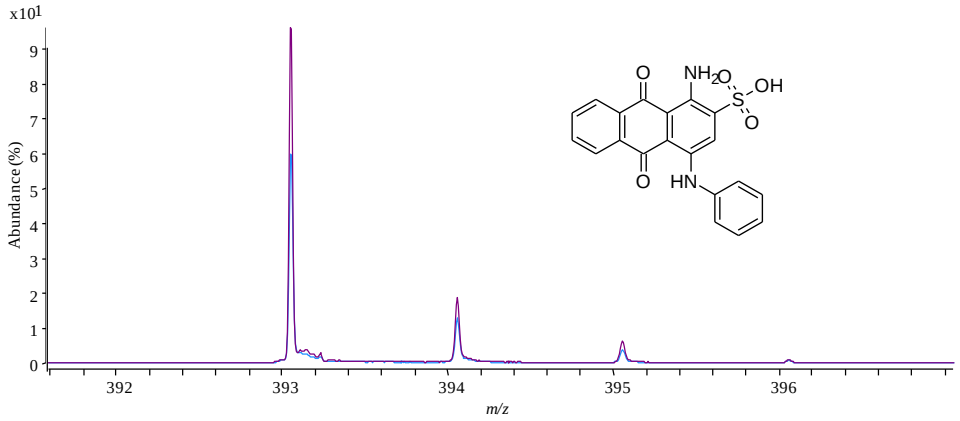

Figure 19. Overlaid MS spectra of C.I. Acid Blue 25 at time points 0-hours (purple) and 40-hours (blue) with the dye structure inset.

5.3 Conclusions

The color chemistry of the dye structure is an important factor when considering light fastness. Azo and anthraquinone dyes are more light fast due to built in chemical properties that help to dissipate the energy while triphenyl-methane dyes tend to be less light fast. Of the 14 dyes compared over the six time points, only one dye, C.I. Acid Green 16, was fully degraded. The addition of stabilizers to the dyes, as is customary for commercial products, also helps to increase photostability and would more closely resemble the types of fibers seen in the forensic laboratory. Other properties such as wash fastness should also be investigated for insight on the potential usefulness of a forensic dye database. The possible degradation due to water and soil exposure would be helpful for fibers found on bodies that have been exposed to the elements. Quantitative analysis of these results was hindered due to sample loss during the extraction procedure.

Chapter 6. Recommendations

At this time, all work discussed has been done utilizing dyed nylon 6,6 prepared in-house or raw dye powders. To truly judge the applicability of the database on real-life samples, the database needs to be expanded to include acid dye samples extracted from commercially dyed products. Commercially dyed products usually contain more than one dye component making the database construction slightly more difficult and time consuming.

In 1994, 44.7% of the fiber used was cellulosic, 27.2% was polyester, 9.6% was polyolefins, 8.6% was polyamides, 5.7% was acryilic, 3.1% was wool, and 1.1% was of

another fiber class entirely *(125)*. The database will need to be expanded to include dyes that are used on the substrates mentions, specifically cellulosic and polyester fibers which encompass 71.9% of the fibers used. To incorporate the other dyes in the LC-MS dye database, methods need to be developed for the extraction and LC-MS analysis of the dye types that do not have existing methods, specifically reactive dyes which are commonly used on cellulose. The expansion of the database to all dye types will be a time consuming and will reinforce the need for a standard database to maintain uniformity and searchability.

Other types of degradation and fastness properties, such as wash fastness, should also be considered for samples that have been exposed to the elements and laundered over time. In forensic cases, fibers will oftentimes be exposed to the elements as well as bacteria and insects. A time lapsed study of dyes extracted from samples exposed to these factors would also be interesting and valuable.

REFERENCES

1. Grieve, M. C.; Biermann, T. W.; Schaub, K., The individuality of fibres used to provide forensic evidence - not all blue polyesters are the same. *Sci. Justice.* **2005,** 45, (1), 13-28.

2. Kiely, T. F., *Forensic Evidence: Science and the Criminal law*. 2nd ed.; CRC Press: Boca Raton, FL, 2006.

3. Grieve, M. C.; Wiggins, K. G., Fibers under fire: suggestions for improving their use to provide forensic evidence. *J Forensic Sci.* **2001,** 46, (4), 835-43.

4. Choudhury, A. K. R., *Textile preparation and dyeing*. Science Publishers: Enfield, NH, 2006; p xiii, 834 p.

5. SWGMAT, Forensic Fiber Examination Guidelines. In 2000.

6. Robertson, J.; Grieve, M.; NetLibrary Inc., *Forensic examination of fibres*. 2nd ed.; CRC Press: Boca Raton, 1999; p 447.

7. Pelton, W. R., Distinguishing the Cause of Textile Fiber Damage Using the Scanning Electron-Microscope (Sem). *J. Forensic Sci.* **1995,** 40, (5), 874-882.

8. Jones, J.; Coyle, T., Automotive flock and its significance in forensic fibre examinations. *Sci. Justice* **2010,** 50, (2), 77-85.

9. De Wael, K., Dichroism measurements in forensic fibre examination. Part 4-dyed acrylic and acetate fibres. *Sci. Justice* **2012,** 52, (2), 81-89.

10. De Wael, K.; Driessche, T. V., Dichroism measurements in forensic fibre examination. Part 2-Dyed polyamide, wool and silk fibres. *Sci. Justice* **2012,** 51, (4), 163-172.

11. De Wael, K.; Lepot, L., Dichroism measurements in forensic fibre examination Part 3-Dyed cotton and viscose fibres. *Sci. Justice* **2012,** 51, (4), 173-186.

12. De Wael, K.; Vanden Driessche, T., Dichroism measurements in forensic fibre examination Part 1-Dyed polyester fibres. *Science & Justice* **2012,** 51, (2), 57-67.

13. Tungol, M. W.; Bartick, E. G.; Montaser, A., The Development of a Spectral Data-Base for the Identification of Fibers by Infrared Microscopy. *Appl. Spectrosc.* **1990,** 44, (4), 543-549.

14. Gal, T.; Ambrus, I.; Urszu, S., Forensic Analysis of Textile Fibers by Fourier-Transform Infrared Diamond Cell Technique. *Acta Chim. Hung.-Mod. Chem.* **1991,** 128, (6), 919-928.

15. Tungol, M. W.; Bartick, E. G.; Montaser, A., Spectral Data-Base for the Identification of Fibers by Infrared Microscopy. *Spectrochim. Acta, Part B* **1991,** 46, (11), E1535-E1544.

16. Kokot, S.; Carswell, S.; Massart, D. L., Application of Drift Spectroscopy for Comparison of Dye Mixtures Extracted from Small Textile Samples. *Appl. Spectrosc.* **1992,** 46, (9), 1393-1399.

17. Tungol, M. W.; Bartick, E. G.; Montaser, A., Forensic Analysis of Acrylic Copolymer Fibers by Infrared Microscopy. *Appl. Spectrosc.* **1993,** 47, (10), 1655-1658.

18. Bartick, E. G.; Tungol, M. W.; Reffner, J. A., A New Approach to Forensic Analysis with Infrared Microscopy - Internal-Reflection Spectroscopy. *Anal. Chim. Acta* **1994,** 288, (1-2), 35-42.

19. Gilbert, C.; Kokot, S., Discrimination of Cellulosic Fabrics by Diffuse-Reflectance Infrared Fourier-Transform Spectroscopy and Chemometrics. *Vibr. Spect.* **1995,** 9, (2), 161-167.

20. Kokot, S.; Crawford, K.; Rintoul, L.; Meyer, U., A DRIFTS study of reactive dye states on cotton fabric. *Vibr. Spect.* **1997,** 15, (1), 103-111.

21. Grieve, M. C.; Griffin, R. M. E.; Malone, R., Characteristic dye absorption peaks found in the FTIR spectra of coloured acrylic fibres. *Sci. Justice.* **1998,** 38, (1), 27-37.

22. Cho, L. L.; Reffner, J. A.; Gatewood, B. M.; Wetzel, D. L., Single fiber analysis by internal reflection infrared microspectroscopy. *J. Forensic Sci.* **2001,** 46, (6), 1309-1314.

23. Ricci, C.; Chan, K. L. A.; Kazarian, S. G., Combining the tape-lift method and Fourier transform infrared spectroscopic imaging for forensic applications. *Appl. Spectrosc.* **2006,** 60, (9), 1013-1021.

24. Bruni, S.; De Luca, E.; Guglielmi, V.; Pozzi, F., Identification of Natural Dyes on Laboratory-Dyed Wool and Ancient Wool, Silk, and Cotton Fibers Using Attenuated Total Reflection (ATR) Fourier Transform Infrared (FT-IR) Spectroscopy and Fourier Transform Raman Spectroscopy. *Appl. Spectrosc.* **2011,** 65, (9), 1017-1023.

25. Minceva-Sukarova, B.; Mangovska, B.; Bogoeva-Gaceva, G.; Petrusevski, V. M., Micro-Raman and Micro-FT-IR Spectroscopic Investigation of Raw and Dyed Pan Fibers. *Croat. Chem. Acta* **2012,** 85, (1), 63-70.

26. Beattie, I. B.; Dudley, R. J.; Smalldon, K. W., Extraction and Classification of Dyes on Single Nylon, Polyacrylonitrile and Polyester Fibers. *J. Soc. Dyers Colour.* **1979,** 95, (8), 295-302.

27. Macrae, R.; Smalldon, K. W., Extraction of Dyestuffs from Single Wool Fibers. *J. Forensic Sci.* **1979,** 24, (1), 109-116.

28. Resua, R., Semi-Micro Technique for the Extraction and Comparison of Dyes in Textile Fibers. *J. Forensic Sci.* **1980,** 25, (1), 168-173.

29. Beattie, I. B.; Roberts, H. L.; Dudley, R. J., Thin-Layer Chromatography of Dyes Extracted from Polyester, Nylon and Polyacrylonitrile Fibers. *Forensic Sci. Int.* **1981,** 17, (1), 57-69.

30. Resua, R.; Deforest, P. R.; Harris, H., The Evaluation and Selection of Uncorrelated Paired Solvent Systems for Use in the Comparison of Textile Dyes by Thin-Layer Chromatography. *J. Forensic Sci.* **1981,** 26, (3), 515-534.

31. Golding, G. M.; Kokot, S., The Selection of Noncorrelated Thin-Layer Chromatographic (TLC) Solvent Systems for the Comparison of Dyes Extracted from Transferred Fibers. *J Forensic Sci.* **1989,** 34, (5), 1156-1165.

32. Grieve, M. C.; Dunlop, J.; Haddock, P., An Investigation of Known Blue, Red, and Black Dyes Used in the Coloration of Cotton Fibers. *J Forensic Sci.* **1990,** 35, (2), 301-315.

33. Rendle, D. F.; Crabtree, S. R.; Wiggins, K. G.; Salter, M. T., Cellulase Digestion of Cotton Dyed with Reactive Dyes and Analysis of the Products by Thin-Layer Chromatography. *J. Soc. Dyers Colour.* **1994,** 110, (11), 338-341.

34. Wiggins, K. G.; Crabtree, S. R.; March, B. M., The importance of thin layer chromatography in the analysis of reactive dyes released from wool fibers. *J. Forensic Sci.* **1996,** 41, (6), 1042-1045.

35. Wiggins, K. G.; Holness, J. A.; March, B. M., The importance of thin layer chromatography and UV microspectrophotometry in the analysis of reactive dyes released from wool and cotton fibers. *J. Forensic Sci.* **2005,** 50, (2), 364-368.

36. Titford, M., Comparison of historic Grubler dyes with modern counterparts using thin layer chromatography. *Biotech. Histochem.* **2007,** 82, (4-5), 227-234.

37. Macrae, R.; Dudley, R. J.; Smalldon, K. W., Characterization of Dyestuffs on Wool Fibers with Special Reference to Microspectrophotometry. *J. Forensic Sci.* **1979,** 24, (1), 117-129.

38. Hartshorne, A. W.; Laing, D. K., The Definition of Color for Single Textile Fibers by Microspectrophotometry. *Forensic Sci. Int.* **1987,** 34, (1-2), 107-129.

39. Suzuki, S.; Suzuki, Y.; Ohta, H.; Sugita, R.; Marumo, Y., Microspectrophotometric discrimination of single fibres dyed by indigo and its derivatives using ultraviolet-visible transmittance spectra. *Sci. Justice* **2001,** 41, (2), 107-111.

40. Eng, M.; Martin, P.; Bhagwandin, C., The Analysis of Metameric Blue Fibers and Their Forensic Significance. *J. Forensic Sci.* **2009,** 54, (4), 841-845.

41. White, P. C.; Munro, C. H.; Smith, W. E., In situ surface enhanced resonance Raman scattering analysis of a reactive dye covalently bound to cotton. *Analyst* **1996,** 121, (6), 835-838.

42. Kokot, S.; Tuan, N. A.; Rintoul, L., Discrimination of reactive dyes on cotton fabric by Raman spectroscopy and chemometrics. *Appl. Spectrosc.* **1997,** 51, (3), 387-395.

43. Keen, I. P.; White, G. W.; Fredericks, P. M., Characterization of fibers by Raman microprobe spectroscopy. *J Forensic Sci.* **1998,** 43, (1), 82-89.

44. White, P. C.; Rodger, C.; Rutherford, V.; Finnon, Y.; Smith, W. E.; Fitzgerald, M., Surface enhanced resonance Raman scattering (SERRS) spectroscopy. A powerful technique for the forensic analysis of colourants? *Invest. Forensic Sci. Tech*. **1999**, 3576, 77-86.

45. Jochem, G.; Lehnert, R. J., On the potential of Raman microscopy for the forensic analysis of coloured textile fibres. *Sci. Justice.* **2002,** 42, (4), 215-221.

46. Massonnet, G.; Buzzini, P.; Jochem, G.; Stauber, M.; Coyle, T.; Roux, C.; Thomas, J.; Leijenhorst, H.; Van Zanten, Z.; Wiggins, K.; Russell, C.; Chabli, S.; Rosengarten, A., Evaluation of Raman Spectroscopy for the analysis of colored fibers: A collaborative study. *J Forensic Sci.* **2005,** 50, (5), 1028-1038.

47. Lepot, L.; De Wael, K.; Gason, F.; Gilbert, B., Application of Raman spectroscopy to forensic fibre cases. *Sci. Justice* **2008,** 48, (3), 109-117.

48. Abbott, L. C.; Batchelor, S. N.; Smith, J. R. L.; Moore, J. N., Resonance Raman and UV-visible spectroscopy of black dyes on textiles. *Forensic Sci. Int.* **2010,** 202, (1-3), 54-63.

49. Zieba-Palus, J.; Was-Gubala, J., An investigation into the use of micro-Raman spectroscopy for the analysis of car paints and single textile fibres. *J. Mol. Struct.* **2011,** 993, (1-3), 127-133.

50. Dockery, C. R.; Stefan, A. R.; Nieuwland, A. A.; Roberson, S. N.; Baguley, B. M.; Hendrix, J. E.; Morgan, S. L., Automated extraction of direct, reactive, and vat dyes from cellulosic fibers for forensic analysis by capillary electrophoresis. *Anal. Bioanal. Chem.* **2009,** 394, (8), 2095-103.

51. Poiger, T.; Richardson, S. D.; Baughman, G. L., Analysis of anionic metallized azo and formazan dyes by capillary electrophoresis-mass spectrometry. *J. Chromatogr. A.* **2000,** 886, (1-2), 259-270.

52. Trojanowicz, M.; Wojcik, L.; Urbaniak-Walczak, K., Identification of natural dyes in historical Coptic textiles by capillary electrophoresis with diode array detection. *Chemia Analityczna* **2003,** 48, (3), 607-620.

53. Fakhari, A. R.; Breadmore, M. C.; Macka, M.; Haddad, P. R., Non-aqueous capillary electrophoresis with red light emitting diode absorbance detection for the analysis of basic dyes. *Anal. Chim. Acta* **2006,** 580, (2), 188-193.

54. Surowiec, I.; Pawelec, K.; Rezeli, M.; Kilar, F.; Trojanowicz, M., Capillary electrophoretic determination of main components of natural dyes with MS detection. *J. Sep. Sci.* **2008,** 31, (13), 2457-2462.

55. Stefan, A. R.; Dockery, C. R.; Baguley, B. M.; Vann, B. C.; Nieuwland, A. A.; Hendrix, J. E.; Morgan, S. L., Microextraction, capillary electrophoresis, and mass spectrometry for forensic analysis of azo and methine basic dyes from acrylic fibers. *Anal. Bioanal. Chem.* **2009,** 394, (8), 2087-94.

56. Stefan, A. R.; Dockery, C. R.; Nieuwland, A. A.; Roberson, S. N.; Baguley, B. M.; Hendrix, J. E.; Morgan, S. L., Forensic analysis of anthraquinone, azo, and metal complex acid dyes from nylon fibers by micro-extraction and capillary electrophoresis. *Anal. Bioanal. Chem.* **2009,** 394, (8), 2077-85.

57. Laing, D. K.; Gill, R.; Blacklaws, C.; Bickley, H. M., Characterization of Acid Dyes in Forensic Fiber Analysis by High-Performance Liquid-Chromatography Using Narrow-Bore Columns and Diode-Array Detection. *J Chrom.* **1988,** 442, 187-208.

58. Griffin, R. M. E.; Speers, S. J.; Elliott, L.; Todd, N.; Sogomo, W.; Kee, T. G., An Improved High-Performance Liquid-Chromatography System for the Analysis of Basic-Dyes in Forensic Casework. *J. Chromatogr., A* **1994,** 674, (1-2), 271-280.

59. Mottaleb, M. A.; Littlejohn, D., Application of an HPLC-FTIR modified thermospray interface for analysis of dye samples. *Anal. Sci.* **2001,** 17, (3), 429-434.

60. Huang, M.; Yinon, J.; Sigman, M. E., Forensic identification of dyes extracted from textile fibers by liquid chromatography mass spectrometry (LC-MS). *J. Forensic Sci.* **2004,** 49, (2), 238-249.

61. Huang, M.; Russo, R.; Fookes, B. G.; Sigman, M. E., Analysis of fiber dyes by liquid chromatography mass spectrometry (LC-MS) with electrospray ionization: Discriminating between dyes with indistinguishable UV-Visible absorption spectra. *J Forensic Sci.* **2005,** 50, (3), 526-534.

62. Petrick, L. M.; Wilson, T. A.; Fawcett, W. R., High-performance liquid chromatography-ultraviolet-visible spectroscopy-electrospray ionization mass spectrometry method for acrylic and polyester forensic fiber dye analysis. *J. Forensic Sci.* **2006,** 51, (4), 771-779.

63. Jandera, P., Selection of separation conditions for HPLC and HPLC/MS of aromatic sulphonic acids and acid azo dyes. *J. Liq. Chromatogr. Relat. Technol.* **2007,** 30, (13-16), 2349-2367.

64. Wheals, B. B., Applications of Pyrolysis Mass Spectrometry(Pyms) to Forensic Problems. *J. Forensic Sci. Soc.* **1984,** 24, (4), 353-353.

65. Tuinman, A. A.; Lewis, L. A.; Lewis, S. A., Trace-fiber color discrimination by electrospray ionization mass spectrometry: A tool for the analysis of dyes extracted from submillimeter nylon fibers. *Anal. Chem.* **2003,** 75, (11), 2753-2760.

66. Soltzberg, L. J.; Hagar, A.; Kridaratikorn, S.; Mattson, A.; Newman, R., MALDI-TOF mass spectrometric identification of dyes and pigments. *J. Am. Soc. Mass Spectrom.* **2007,** 18, (11), 2001-2006.

67. Hiroma, Y.; Hokura, A.; Nakai, I., Forensic Identification of Trunk Mat by Trace Element Analysis of Single Fiber with Laser Ablation ICP-MS. *Bunseki Kagaku* **2010,** 59, (9), 759-769.

68. Lovejoy, K. S.; Purdy, G. M.; Iyer, S.; Sanchez, T. C.; Robertson, A.; Koppisch, A. T.; Del Sesto, R. E., Tetraalkylphosphonium-Based Ionic Liquids for a Single-Step Dye Extraction/MALDI MS Analysis Platform. *Anal. Chem.* **2011,** 83, (8), 2921-2930.

69. Grieve, M. C.; Dunlop, J.; Haddock, P., An Assessment of the Value of Blue, Red, and Black Cotton Fibers as Target Fibers in Forensic-Science Investigations. *J Forensic Sci.* **1988,** 33, (6), 1332-1344.

70. Wiggins, K. G.; Cook, R.; Turner, Y. J., Dye Batch Variation in Textile Fibers. *J. Forensic Sci.* **1988,** 33, (4), 998-1007.

71. Palmer, R.; Chinherende, V., A target fiber study using cinema and car seats as recipient items. *J Forensic Sci.* **1996,** 41, (5), 802-803.

72. Taupin, J. M., Hair and fiber transfer in an abduction case - Evidence from different levels of trace evidence transfer. *J. Forensic Sci.* **1996,** 41, (4), 697-699.

73. Kelly, E.; Griffin, R. M. E., A target fibre study on seats in public houses. *Sci. Justice* **1998,** 38, (1), 39-44.

74. Grieve, M. C.; Biermann, T.; Davignon, M., The occurrence and individuality of orange and green cotton fibres. *Sci. Justice* **2003,** 43, (1), 5-22.

75. Grieve, M. C.; Biermann, T. W., The individuality of blue polyester fibers used to provide forensic evidence. *Forensic Sci. Int.* **2003,** 136, 121-122.

76. Wiggins, K.; Drummond, P., The analysis and comparison of blue wool fibre populations found at random on clothing. *Sci. Justice* **2005,** 45, (3), 157-162.

77. Wiggins, K.; Holness, J. A., A further study of dye batch variation in textile and carpet fibres. *Sci. Justice* **2005,** 45, (2), 93-96.

78. Biermann, T. W., Blocks of colour IV: The evidential value of blue and red cotton fibres. *Sci. Justice* **2007,** 47, (2), 68-87.

79. Palmer, R.; Hutchinson, W.; Fryer, V., The discrimination of (non-denim) blue cotton. *Sci. Justice* **2009,** 49, (1), 12-18.

80. Jones, J.; Coyle, T., Synthetic flock fibres: A population and target fibre study. *Sci. Justice* **2011,** 51, (2), 68-71.

81. Saferstein, R., *Forensic science handbook*. 2nd ed.; Prentice Hall: Upper Saddle River, NJ, 2002; Vol. II, p 231-289.

82. Skoog, D. A.; Holler, F. J.; Crouch, S. R., *Principles of instrumental analysis*. 6th ed.; Thomson Brooks/Cole: Belmont, CA, 2007; p 1039.

83. Standard Guide for Forensic Examination of Non-Reactive Dyes in Textile Fibers by Thin-Layer Chromatography. In ASTM International 2008.

84. Snyder, L. R.; Kirkland, J. J.; Dolan, J. W., *Introduction to modern liquid chromatography*. 3rd ed.; Wiley: Hoboken, N.J., p. 912 .

85. Storm, T.; Reemtsma, T.; Jekel, M., Use of volatile amines as ion-pairing agents for the high-performance liquid chromatographic-tandem mass spectrometric determination of aromatic sulfonates in industrial wastewater. *J. Chromatogr., A* **1999,** 854, (1-2), 175-185.

86. Watson, J. T.; Sparkman, O. D., *Introduction to Mass Spectrometry*. 4th ed. ed.; John Wiley & Sons Ltd: West Sussex, 2007.

87. Ardrey, R. E., *Liquid chromatography-mass spectrometry : an introduction*. J. Wiley: New York, 2003; p 75-100.

88. Dole, M.; Mack, L. L.; Hines, R. L., Molecular Beams of Macroions. *J. Chem. Phys.* **1968,** 49, (5), 2240-2250.

89. Iribarne, J. V.; Thomson, B. A., Evaporation of Small Ions from Charged Droplets. *Trans.-Am. Geophys. Union* **1975,** 56, (12), 992-993.

90. Kebarle, P.; Verkerk, U. H., Electrospray: from Ions in Solution to Ions in the Gas Phase, What We Know Now. *Mass Spectrom. Rev.* **2009,** 28, (6), 898-917.

91. Dass, C., *Fundamentals of contemporary mass spectrometry*. Wiley-Interscience: Hoboken, N.J., 2007; p 80-86.

92. Comisarow, M. B., Theory of Fourier-Transform Ion-Cyclotron Resonance Mass-Spectroscopy .2. Signal Modeling for Ion-Cyclotron Resonance. *J. Chem. Phys.* **1978,** 69, (9), 4097-4104.

93. Makarov, A.; Denisov, E.; Lange, O.; Horning, S., Dynamic range of mass accuracy in LTQ Orbitrap hybrid mass spectrometer. *J. Am. Soc. Mass Spectrom.* **2006,** 17, (7), 977-982.

94. Olsen, J. V.; de Godoy, L. M. F.; Li, G. Q.; Macek, B.; Mortensen, P.; Pesch, R.; Makarov, A.; Lange, O.; Horning, S.; Mann, M., Parts per million mass accuracy on an orbitrap mass spectrometer via lock mass injection into a C-trap. *Molecular & Cellular Proteomics* **2005,** 4, (12), 2010-2021.

95. Hu, Q. Z.; Noll, R. J.; Li, H. Y.; Makarov, A.; Hardman, M.; Cooks, R. G., The Orbitrap: a new mass spectrometer. *J. Mass Spectrom.* **2005,** 40, (4), 430-443.

96. Olsen, J. V.; de Godoy, L. M. F.; Li, G. Q.; Macek, B.; Mortensen, P.; Pesch, R.; Makarov, A.; Lange, O.; Horning, S.; Mann, M., Parts per million mass accuracy on an orbitrap mass spectrometer via lock mass injection into a C-trap. *Mol. Cell. Proteom.* **2005,** 4, (12), 2010-2021.

97. Han, J.; Danell, R. M.; Patel, J. R.; Gumerov, D. R.; Scarlett, C. O.; Speir, J. P.; Parker, C. E.; Rusyn, I.; Zeisel, S.; Borchers, C. H., Towards high-throughput metabolomics using ultrahigh-field Fourier transform ion cyclotron resonance mass spectrometry. *Metabolomics* **2008,** 4, (2), 128-140.

98. Kind, T.; Fiehn, O., Metabolomic database annotations via query of elemental compositions: Mass accuracy is insufficient even at less than 1 ppm. *Bmc Bioinformatics* **2006,** 7, 234.

99. Grange, A. H.; Donnelly, J. R.; Sovocool, G. W.; Brumley, W. C., Determination of elemental compositions from mass peak profiles of the molecular ion (M) and the M+1 and M+2 ions. *Anal. Chem.* **1996,** 68, (3), 553-560.

100. Erve, J. C. L.; Gu, M.; Wang, Y. D.; DeMaio, W.; Talaat, R. E., Spectral Accuracy of Molecular Ions in an LTQ/Orbitrap Mass Spectrometer and Implications for Elemental Composition Determination. *J. Am. Soc. Mass Spectrom.* **2009,** 20, (11), 2058-2069.

101. Xu, Y.; Heilier, J. F.; Madalinski, G.; Genin, E.; Ezan, E.; Tabet, J. C.; Junot, C., Evaluation of Accurate Mass and Relative Isotopic Abundance Measurements in the LTQ-Orbitrap Mass Spectrometer for Further Metabolomics Database Building. *Anal. Chem.* **2010,** 82, (13), 5490-5501.

102. Stoll, N.; Schmidt, E.; Thurow, K., Isotope pattern evaluation for the reduction of elemental compositions assigned to high-resolution mass spectral data from electrospray ionization Fourier transform ion cyclotron resonance mass spectrometry. *J. Am. Soc. Mass Spectrom.* **2006,** 17, (12), 1692-1699.

103. Bohlke, J. K.; de Laeter, J. R.; De Bievre, P.; Hidaka, H.; Peiser, H. S.; Rosman, K. J. R.; Taylor, P. D. P., Isotopic compositions of the elements, 2001. *J. Chem. Phys. Ref. Data* **2005,** 34, (1), 57-67.

104. Shi, S. D. H.; Hendrickson, C. L.; Marshall, A. G., Counting individual sulfur atoms in a protein by ultrahigh-resolution Fourier transform ion cyclotron resonance mass spectrometry: Experimental resolution of isotopic fine structure in proteins. *Proc. Natl. Acad. Sci. USA* **1998,** 95, (20), 11532-11537.

105. Hoye, T. R.; Dvornikovs, V.; Fine, J. M.; Anderson, K. R.; Jeffrey, C. S.; Muddiman, D. C.; Shao, F.; Sorensen, P. W.; Wang, J., Details of the structure determination of the sulfated steroids PSDS and PADS: New components of the sea lamprey (Petromyzon marinus) migratory pheromone. *J. Org. Chem.* **2007,** 72, (20), 7544-7550.

106. He, H., **2010,** Int. J. Mass Spectrom., (doi:10.1016/j.ijms.2010.10.014).

107. Belov, M. E.; Zhang, R.; Strittmatter, E. F.; Prior, D. C.; Tang, K.; Smith, R. D., Automated gain control and internal calibration with external ion accumulation capillary liquid chromatography-electrospray ionization-fourier transform ion cyclotron resonance. *Anal. Chem.* **2003,** 75, (16), 4195-4205.

108. Syka, J. E. P.; Marto, J. A.; Bai, D. L.; Horning, S.; Senko, M. W.; Schwartz, J. C.; Ueberheide, B.; Garcia, B.; Busby, S.; Muratore, T.; Shabanowitz, J.; Hunt, D. F., Novel Linear Quadrupole Ion Trap/FT Mass Spectrometer: Performance

Characterization and Use in the Comparative Analysis of Histone H3 Post-translational Modifications. *Journal of Proteome Research* **2004,** 3, 621-626.

109. Williams, D. K.; Muddiman, D. C., Parts-per-billion mass measurement accuracy achieved through the combination of multiple linear regression and automatic gain control in a Fourier transform ion cyclotron resonance mass spectrometer. *Anal. Chem.* **2007,** 79, (13), 5058-5063.

110. Manly, B. F. J., *Multivariate statistical methods : a primer*. Chapman and Hall: London ; New York, 1986; p 159.

111. Muehlethaler, C.; Massonnet, G.; Esseiva, P., The application of chemometrics on Infrared and Raman spectra as a tool for the forensic analysis of paints. *Forensic Sci. Int.* 209, (1-3), 173-82.

112. Ryder, A. G., Classification of narcotics in solid mixtures using principal component analysis and Raman spectroscopy. *J Forensic Sci.* **2002,** 47, (2), 275-84.

113. Klemenc, S., In common batch searching of illicit heroin samples--evaluation of data by chemometrics methods. *Forensic Sci. Int.* **2001,** 115, (1-2), 43-52.

114. Thanasoulias, N. C.; Piliouris, E. T.; Kotti, M. S.; Evmiridis, N. P., Application of multivariate chemometrics in forensic soil discrimination based on the UV-Vis spectrum of the acid fraction of humus. *Forensic Sci. Int.* **2002,** 130, (2-3), 73-82.

115. Kher, A. A.; Green, E. V.; Mulholland, M. I., Evaluation of principal components analysis with high-performance liquid chromatography and photodiode array detection for the forensic differentiation of ballpoint pen inks. *J. Forensic Sci.* **2001,** 46, (4), 878-83.

116. Senko, M. W.; Beu, S. C.; Mclafferty, F. W., Determination of Monoisotopic Masses and Ion Populations for Large Biomolecules from Resolved Isotopic Distributions. *J. Am. Soc. Mass Spectrom.* **1995,** 6, (4), 229-233.

117. Makarov, A., In 2011.

118. Perry, R. H.; Cooks, R. G.; Noll, R. J., Orbitrap Mass Spectrometry: Instrumentation, Ion Motion and Applications. *Mass Spectrom. Rev.* **2008,** 27, (6), 661-699.

119. Hofstadler, S. A.; Bruce, J. E.; Rockwood, A. L.; Anderson, G. A.; Winger, B. E.; Smith, R. D., Isotopic Beat Patterns in Fourier Transform Ion Cyclotron Resonance Mass Spectrometry: Implications for High Resolution Mass Measurements of Large Biopolymers. *Int. J. Mass Spectrom. Ion Processes* **1994,** 132, 109-127.

120. Gordon, E. F.; Muddiman, D. C., Impact of ion cloud densities on the measurement of relative ion abundances in Fourier transform ion cyclotron resonance mass spectrometry: experimental observations of coulombically induced cyclotron radius perturbations and ion cloud dephasing rates. *J. Mass Spectrom.* **2001,** 36, 195-203.

121. Blake, S. L.; Walker, S. H.; Muddiman, D. C.; Hinks, D.; Beck, K. R., Spectral Accuracy and Sulfur Counting Capabilities of the LTQ-FT-ICR and the LTQ-Orbitrap XL for Small Molecule Analysis. *J. Am. Soc. Mass Spectrom.* **2011,** 22, (12), 2269-2275.

122. Society of Dyers and Colourists.; American Association of Textile Chemists and Colorists., *Colour index international*. 3rd ed.; The Society: Bradford, West Yorkshire, 1987.

123. Freeman, H. S.; Posey, J. C., An Approach to the Design of Lightfast Disperse Dyes - Analogs of Disperse Yellow-42. *Dyes Pigm.* **1992,** 20, (3), 171-195.

124. Allen, N. S., Photofading and Light-Stability of Dyed and Pigmented Polymers. *Polym. Degrad. Stab.* **1994,** 44, (3), 357-374.

125. Choudhury, A. K. R., *Textile preparation and dyeing*. Science Publishers: Enfield, NH, 2006; p 632-655.